Materials Science and Engineering R 113 (2017) 1–29

Contents lists available at ScienceDirect

Materials Science and Engineering R

journal homepage: www.elsevier.com/locate/mser

Processing-structure-property relationships of continuous carbon fiber polymer-matrix composites

D.D.L. Chung[1]

Composite Materials Research Laboratory,Department of Mechanical and Aerospace Engineering, University at Buffalo, The State University of New York, Buffalo, NY 14260-4400, USA

ARTICLE INFO

Article history:
Received 1 September 2016
Accepted 16 January 2017
Available online xxx

Keywords:
Carbon fiber
Polymer-matrix composite
Processing
Structure
Properties
Applications

ABSTRACT

This paper reviews the processing-structure-property relationships of continuous carbon fiber polymer-matrix composites, which are important for lightweight structures. Such relationships constitute the guiding principles in materials design, development and tailoring. Although much research has been performed for decades on the mechanical behavior of continuous fiber composites, the functional behavior (electrical, electromagnetic, dielectric, thermal, thermoelectric, vibration damping, etc.) of these materials are quite new, with research activities that are rapidly growing in recent years due to the importance of multifunctional structural materials and smart structures. In addition, the combined use of continuous fibers and nanofillers such as nanofibers and nanotubes is a relatively new direction that has provided hierarchical or multi-scale composites with attractive properties. The properties addressed in this review relate to the mechanical (static, dynamic, fatigue, wear), viscoelastic, thermal expansion, thermal conductivity, electrical, piezoresistive, dielectric, electromagnetic, thermoelectric and environmental durability behavior, as well as the effects of temperature, humidity, strain and damage. The structure/processing parameters relate to the fiber arrangement, interlaminar interface, curing pressure, fiber type, fiber treatments, fiber volume fraction, fillers, interlayers, coatings, through-thickness rods, polymer matrix and the fastening-relevant interface between contacting unbonded composites. In addition, this paper reviews the rapidly broadening applications of this class of materials.

Contents

[1] http://alum mit ed foru/www/ddlchung.

http://dx.doi.org/10.1016/j.mser.2017.01.002
0927-796X/

1. Introduction

Processing governs the structure of a material. The structure in term governs the properties of the material. The processing-structure-property relationships constitute the guiding principles in materials design, development and tailoring, and represent the core of materials science and engineering. This core in the context of metallurgy has long been established. However, this core in the context of non-metallic materials has not been addressed adequately.

Composite materials refer to artificial combinations of materials, such that a certain material is the matrix and certain other material is the filler (whether continuous or discontinuous). The processing-structure-property relationships of composite materials have not been addressed adequately, particularly in relation to properties other than the mechanical properties.

Due to their combination of low density, high strength and high elastic modulus, continuous carbon fibers are dominant among reinforcements used for high-performance lightweight composite materials, particularly polymer-matrix composites. The dominance of polymer-matrix composites among composites with various matrices (polymer, carbon, ceramic, metal, cement, etc.) stems from the relative ease (low cost) of fabrication and the relatively good bonding ability of polymers. Applications include aircraft, satellites, automobile, sporting goods, wind turbines, structural repair, etc.

Much investigation has been performed over decades on the mechanical behavior of continuous fiber polymer-matrix composites and mechanics-based theories for explaining the mechanical behavior are well established. However, the functional behavior (electrical, electromagnetic, dielectric, thermal, thermoelectric, vibration damping, etc.) of these materials are relatively new, with research activities that are rapidly growing in recent years due to

the rising importance of multifunctional structural materials and smart structures. In addition, the combined use of continuous fibers and nanofillers such as nanofibers and nanotubes in the same composite is a relatively new direction that has provided hierarchical (multi-scale) composites with attractive properties.

Continuous carbon fibers refer to conventional carbon fibers that consist essentially entirely of carbon in the graphite family (with sp2 hybridization of the carbon atoms), such that the carbon is a continuous phase throughout the length of the fiber. The carbon in a continuous carbon fiber is typically non-crystalline (a form known as turbostratic carbon), though a degree of crystallinity can be present if the fiber has been heat treated at a high temperature above 2000 °C. Although turbostratic carbon is non-crystalline, it consists of carbon layers that are limited in the degrees of parallelism and flatness and in the in-plane and out-of-plane dimensions of the carbon layer stack.

Continuous carbon fibers are to be distinguished from continuous yarns. A yarn consists of discontinuous fibers, nanofibers, nanotubes or graphene flakes that cling to one another through van der Waals' forces. The tensile strength of a carbon nanotube (CNT) yarn is limited by the low strength of the interface between CNT bundles in the yarn and by the porosity in the yarn.

This paper is a review that addresses the processing-structure-property relationships of continuous carbon fiber polymer-matrix composites. The properties relate to the mechanical, viscoelastic, thermal expansion, thermal conductivity, electrical, dielectric, electromagnetic, thermoelectric and environmental durability behavior, as well as the effects of temperature, strain and damage. In addition, this paper reviews the rapidly broadening applications of this class of materials.

High strength and modulus are obviously important for load bearing. Viscoelastic behavior is relevant to vibration damping. A tailored coefficient of thermal expansion (CTE) is attractive for thermal stress reduction and thermal fatigue resistance. High thermal conductivity is attractive for heat dissipation, as needed for aircraft and electronics. Electrical conductivity is attractive for resistive heating (Joule heating, with applications such as the deicing of aircraft and wind turbines), lightning protection, electrical grounding and electrical-resistance-based self-sensing. Dielectric behavior (pertaining to the electric permittivity and electrical energy loss) relates to the AC electrical behavior, which is important for numerous electrical devices, such as batteries, capacitors, etc. Electromagnetic behavior is relevant to electromagnetic interference (EMI) shielding and low observability (with applications such as Stealth aircarft). Thermoelectric behavior is relevant to the generation of electricity (renewable energy) from waste heat.

2. Carbon fibers vs. other continuous fibers

Carbon, glass (silicate) and aramid (Kevlar, a polyamide in which all the amide groups are separated by para-phenylene) fibers are the three main types of structural fibers. As shown in Table 1, the compressive strength of carbon fiber is lower than that of glass fiber. For carbon fiber, the tensile strength is much higher than the compressive strength. The tensile strain at failure (the ductility) is considerably lower for carbon fiber than glass or Kevlar fiber. For all three types of fiber, the strain at failure is much lower than that of steel.

The CTE along the fiber axis is negative for carbon fiber and Kevlar fiber, but is positive for glass fiber. The negative CTE of carbon fiber is due to the carbon in-plane interatomic bond distance increasing as the temperature increases; this bond distance increase is accompanied by an increase in the degree of waviness of the layers. As a consequence of the increased waviness, the carbon layers are shortened. The fact that the axial CTE of carbon fiber is negative is consistent with the fact that the in-plane CTE of graphite is negative at temperatures below 400 °C. The negative value is a consequence of the lattice vibrational modes of graphite [1]. The higher is the temperature, the greater is the amplitude of the thermal vibration. An asymmetry in the extent of inward and outward vibration of the atoms that make up a bond gives rise to a change in the average bond distance as the temperature increases and hence the phenomenon of thermal expansion. The negative CTE of Kevlar fiber is similarly due to the long polyamide molecules becoming wavier in the molecular configuration, in spite of the increase in interatomic bond distance, as the temperature increases. The axial CTE is much more negative for Kevlar fiber than carbon fiber, due to the greater ease of bending for a molecule than a carbon layer. For all three types of fiber, the CTE magnitude is much lower than that of steel.

Compared to glass fiber and Kevlar fiber, carbon fiber is clearly advantageous is the high tensile modulus, and the low magnitude of the CTE. Additional advantages that are not shown in Table 1 are the high temperature resistance, chemical resistance, electrical conductivity and thermal conductivity. The electrical/thermal conductivity is advantageous for some applications (e.g., lightning protection, electrostatic energy harvesting, EMI shielding, resistance heating, microelectronic heat sinks and thermal straps), but is disadvantageous for some other applications (e.g., printed circuit boards that require electrical insulation ability).

3. Structure of continuous carbon fiber polymer-matrix composites

The structure of continuous carbon fiber polymer-matrix composites pertains mainly to the fiber arrangement (including

Table 1
Comparison of the basic properties of carbon fiber, glass fiber and Kevlar fiber and carbon steel. There are various grades of each type of fiber. A commonly used grade is chosen to represent each type of fiber. The data are from the manufacturers' datasheets, unless stated otherwise.

Property	Carbon fiber (T300)	Glass fiber (S-2)	Kevlar fiber (49)	Carbon steel (not fiber)
Density (g/cm^3)	1.76	2.46	1.45	7.85
Tensile modulus (GPa)	230	86.9	112	190–210
Specific tensile modulus (GPa.cm^3/g)	131	35.3	77.2	24.2–26.8
Tensile strength (GPa)	3.53	4.89	3.00	0.276–1.882
Specific tensile strength (GPa.cm^3/g)	2.010	1.990	2.070	0.035–0.24
Tensile strain (ductility)	1.5%	5.7%	2.4%	10%–32%
Compressive strength (GPa)	0.87[a]	1.60	/	/
CTE[b] (axial, 10^{-6}/K)	−0.41	2.9	−6	11.0–16.6

[a] Calculated value [190].
[b] CTE = coefficient of thermal expansion.

the fiber lay-up configuration), the interlaminar interface and the fiber weaving configuration (if applicable), as described in this section. Additional structural aspects are addressed in Sec. 4.

3.1. Fiber arrangement

Continuous carbon fiber polymer-matrix composites are primarily of one of several forms. These forms include multidirectional fiber laminates (made by the stacking and consolidation of fiber laminae, with the fibers in each lamina being either unidirectional or woven and the number of fibers stacked along the thickness of each lamina typically ranging from 25 to 50), unidirectional fiber rods (made by pultrusion) and multidirectionally wound fiber tubings (made by filament winding). In all of these forms, the composite is highly anisotropic, with the strength, modulus, electrical conductivity and thermal conductivity [2] being all much higher in the fiber direction of the composite than the other directions.

In the fabrication of continuous carbon fiber polymer-matrix composites, the lay-up process is most common and involves the stacking of laminae (plies) of carbon fibers in prescribed fiber orientations for the different lies. The fiber orientation is the same for the fibers in the same lamina, but tends to differ for the fibers in different laminae. The choice of the fiber orientations allows tailoring of the composite mechanical properties as required by specific applications. The lay-up configuration of the laminae greatly affects the mechanical properties (strength, modulus, toughness, etc.) of the composite [3].

Although the unidirectional geometry involves ideally all the fibers being aligned and parallel to one another, the fibers are always slightly wavy, with the deviation from straightness in both the through-thickness and transverse directions. Due to the anisotropy of a fiber, the waviness (known as marcelling) is not attractive for the mechanical performance of the composite. However, it results in a degree of fiber–fiber contact both in the transverse in-plane direction and the through-thickness direction (Fig. 1).

For high-performance structural applications, the laminates involve non-woven fibers, such that the fibers are unidirectional in each lamina and the fiber directions in different laminae are not all the same. By having a number of different fiber directions for different laminae, the overall composite exhibits adequate mechanical properties in various directions in the plane of the laminate. By proper selection of these directions, as in Fig. 2, the mechanical properties may approach isotropy in the plane of the laminate. The lay-up configuration illustrated in Fig. 2 is said to be quasi-isotropic. However, the mechanical properties are poor in the direction perpendicular to this plane, due to the weak link at the interlaminar interface. The fiber volume fraction in a laminate is preferably high, since the fibers are the load-bearing component. Hence, the fiber volume fraction is typically about 60%.

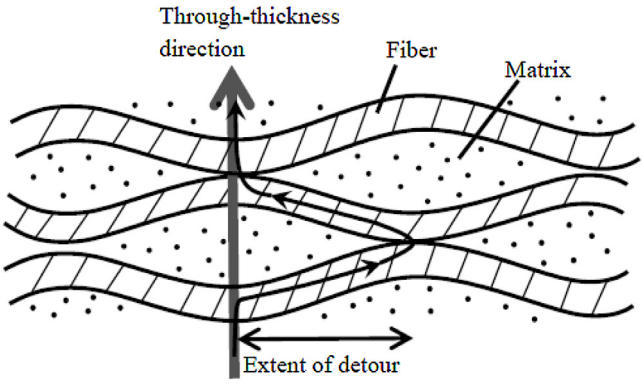

Fig 1. Fiber waviness resulting in fiber–fiber contact. This illustration shows the fiber–fiber contact along the thickness direction. The contact occurs at points and results in the electrical/thermal conduction path detouring to reach a contact point. [4].

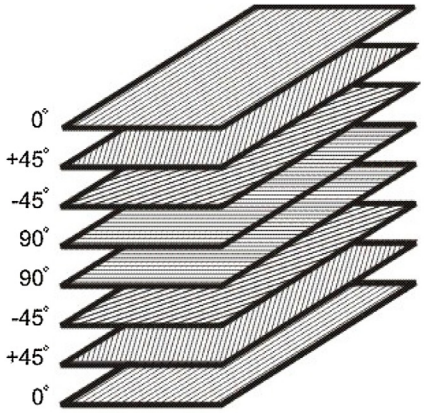

(a)

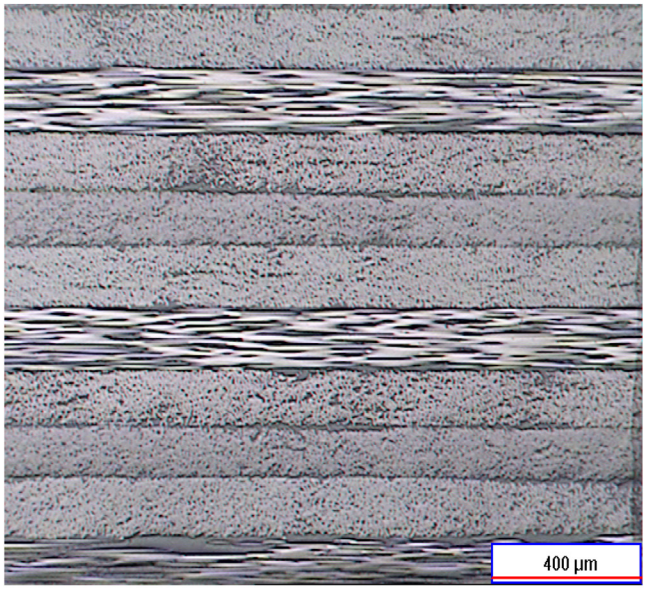

(b)

Fig. 2. (a) An example of a fiber lay-up configuration of a multidirectional laminate. This configuration gives mechanical properties that are roughly isotropic in the plane of the laminate. (http://www.composites.ugent.be/home_made_composites/what_are_composites.html, public domain) (b) Optical microscope photograph of the mechanically polished cross-section of a 24-lamina continuous carbon fiber epoxy-matrix composite with a quasi-isotropic fiber lay-up configuration $[0/45/90/-45]_{3s}$. The relatively bright laminae are the 0° laminae. [4].

Continuous fibers are available in the form of bundles, which are known as tows. The number of fibers in a tow varies, but is typically in the thousands or tens of thousands. This number is commonly indicated such that, for example, tows with 12,000 fibers in a tow are designated 12 K. A tow may have its fibers spread out and aligned mechanically to form a sheet, such that the number of fibers stacked along the thickness of the sheet (typically 20–50) is much smaller than the number of fibers in a tow. Tows with the fibers spread out and aligned can be used to form a ply (known as a lamina) in the resulting laminate. The larger is the number of fibers in a tow, the thicker tends to be a lamina. Alternately, tows can have its fibers similarly spread out and aligned to form a ribbon (known as a tape), which can be wound on

an object (called the mandrel) to form a composite in the form of a cylinder or hollow rod with a selected cross-sectional shape.

Tows (without the fibers in a tow spread out) can be woven together to form cloth or fabric, or be braided to form a tube. There are various configurations of weaving. The weaving involves the fibers in two or more directions, so that the resulting fabric has adequate mechanical properties in multiple directions. Weaving is commonly conducted in two dimensions (2D). However, three-dimensional (3D) weaving is increasingly common. The classical form of 3D fabric involves using one or more fibers in each of the three dimensions during the weaving. A relatively simple form of 3D fabric involves stitching 2D woven fabric sheets together. A composite is commonly made from a stack of 2D woven fabric. Such a composite is strong in the plane of the fabric, but is weak in the direction perpendicular to this plane. In contrast, a 3D woven structure can be mechanically good in all three directions in terms of the mechanical properties and the thermal conductivity [5–7].

The tow may break if its radius of curvature during the weaving is too small [8]. Nevertheless, the fabric form is convenient to handle, as it is more sturdy mechanically and easier to handle than a sheet of aligned fibers. Even if a binder is present, a sheet of aligned fibers is weak in the direction perpendicular to the fibers. On the other hand, the fibers in a fabric are necessarily bent, since weaving involves having fibers overlapping and bending around one another. Due to the fact that the fiber properties are superior along the fiber axis than the transverse direction and due to the sites of stress concentration resulting from the bending, the bending affects the composite properties negatively. Therefore, fabrics are typically not used for high-performance structural composites (e.g., aircraft structures), which use sheets of aligned fibers instead. However, fabrics are used for less demanding applications, such as bicycle components.

Carbon fibers in the continuous form are used mainly as the reinforcement in polymer-matrix composites. Composites with carbon matrices are important for high-temperature structures, such as aircraft brakes. Epoxy is the most common polymer matrix for carbon fiber composites, due to its high adhesiveness and longstanding use in composites. However, thermoplastic matrices are increasingly important, due to their toughness and other attractions.

Fig. 2(b) shows an optical microscope photograph of a mechanically polished cross-section of a carbon fiber epoxy-matrix composite laminate that consists of a number of fiber laminae stacked up and bonded together by the matrix, such that the orientation of the fibers are the same in each lamina but adjacent laminae have fibers that are oriented along different directions. In general, the various laminae can have a variety of different fiber orientations, as needed to tailor the properties of the composite. A particularly common lay-up configuration involves four fiber directions, i.e., [0/90/+45/-45], and is known as the quasi-isotropic configuration, due to the two-dimensional isotropy (approximate) in the plane of the laminae. In order to avoid warpage of the laminate (resulting from the difference in coefficient of thermal expansion, CTE, of the laminae with fibers oriented in different directions), the lay-up configuration is preferably symmetrical relative to the mid-plane of the laminate. Thus, the quasi-isotropic configuration with 8 laminae can have the lay-up configuration [0/90/+45/-45/-45/+45/90/0] or [0/+45/-45/90/90/-45/+45/0], for example, so that the top four laminae and the bottom four laminae are mirror images of one another, with the mirror plane being at the center of the laminate.

The presence of a carbon filler can affect the curing of a resin. As shown for an epoxy resin (specifically one with a linear amine curing agent), the presence of a carbon filler increases the heat of the curing reaction, especially if the filler is ozone-treated carbon fiber (with oxygen-containing surface functional groups resulting from the ozone treatment). Ozone-treated carbon fiber increases the heat of curing more than carbon nanofiber (originally known as carbon filament) or carbon black. The presence of a carbon filler also accelerates the curing reaction, especially if the filler is carbon black (with a relatively high specific surface area due to the nanostructure). Carbon black accelerates the curing process more than carbon nanofiber or carbon fiber. Increasing the specific surface area of a carbon filler accelerates the curing of epoxy, but it has a negligible effect on the heat of the curing reaction. Activation is a reaction process that greatly increases the surface porosity. As a result, activated carbon exhibits high specific surface area. Ozone-treatment increases the heat of curing of epoxy filled with carbon fiber more than activation, but it accelerates the curing less than activation. [9]

Table 2
Effect of curing pressure on the structure of 7-lamina crossply continuous carbon fiber epoxy-matrix composite. The interlaminar interface thickness and the lamina thickness essentially do not vary with the number of laminae. [10].

Property	Curing pressure (MPa)	
	0.5	2.0
Interlaminar interface thickness (μm)	8.1 ± 3.1	3.2 ± 1.5
Lamina thickness (μm)	139.8 ± 7.4	130.5 ± 6.5
Fiber volume fraction	0.579 ± 0.020	0.656 ± 0.023
Matrix volume fraction	0.421 ± 0.019	0.344 ± 0.023
Composite thickness (μm)	1020 ± 50	930 ± 40
Composite density (g/cm^3)	1.583 ± 0.005	1.630 ± 0.014
Loss tangent[a]	0.0086 ± 0.0002	0.0079 ± 0.0001
Storage modulus (GPa)[a]	127.8 ± 1.7	160.7 ± 8.1
Loss modulus (GPa)[a]	1.10 ± 0.04	1.28 ± 0.06

[a] Based on dynamic flexural testing at 0.2 Hz (three-point bending, sinusoidal).

Table 2 shows the basic structural parameters of continuous carbon fiber epoxy-matrix composites and the effect of the curing pressure on these parameters. The fiber volume fraction is around 60%, being slightly higher for the higher curing pressure. Hence, the matrix volume fraction is around 40%. The lamina thickness is around 130 μm, being very slightly (if at all) lower for the higher curing pressure. The associated interlaminar interface thickness is a few micrometers, being substantially lower for the higher curing pressure.

The abovementioned lamina thickness and interlaminar interface thickness just constitute an example. The values vary greatly, because of the variation in the number of fibers per tow. A larger tow size tends to be associated with larger values of the lamina thickness and interlaminar interface thickness.

As shown in Table 2, the composite density is 1.6 g/cm^3, being slightly higher for the higher curing pressure. The composite thickness is very slightly (if at all) lower for the higher curing pressure. The flexural storage modulus is substantially higher for the higher curing pressure, due to the high modulus of the fiber and the dominance of the fiber in governing the flexural behavior. The loss tangent (tan δ, which describes the degree of viscous character, with $\delta = 0^\circ$ for purely elastic behavior and $\delta = 90^\circ$ for purely viscous behavior) is low, at around 0.008, due to the dominance of the fiber in governing the flexural behavior; the value is lower for the higher curing pressure, due to the lower matrix volume fraction and the matrix being the primary contributor to the viscous character of the composite. The loss modulus (equal to the product of the loss tangent and the storage modulus) is low, at around 1.1 GPa, due to the low degree of viscous character; its value is slightly higher for the lower curing pressure. Please refer to Sec. 4.7.2 for more detailed coverage of the viscoelastic behavior.

The interlaminar interface refers to the interface between the laminae in a fiber laminate. Fig. 3 shows optical microscope photographs of the mechanically polished cross-section of a

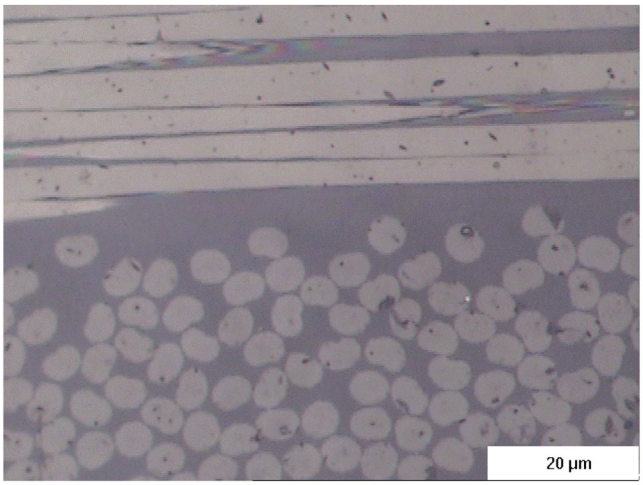

(a)

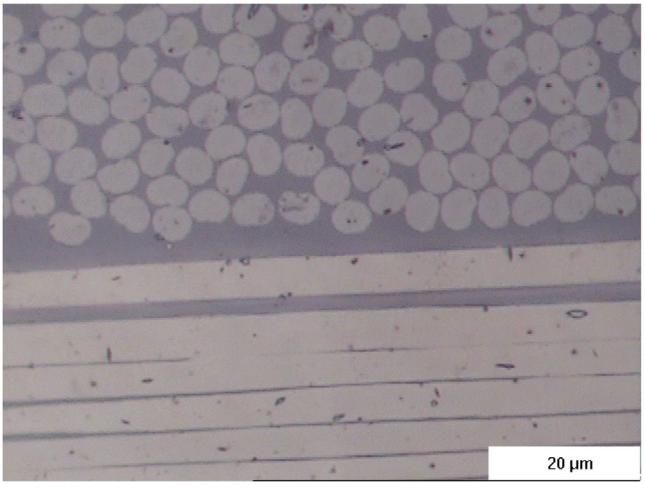

(b)

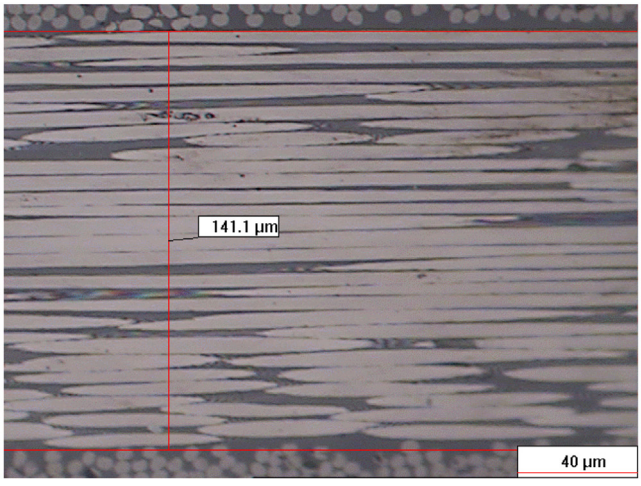

(c)

Fig. 3. Optical microscope photographs of the cross-section of continuous carbon fiber epoxy-matrix composites. (a) Composite fabricated at a curing pressure of 0.5 MPa, showing parts of two laminae and the interlaminar interface between them. The fibers in the two laminae are oriented 90° apart. (b) Composite fabricated at a curing pressure of 2.0 MPa, showing parts of two laminae and the interlaminar interface between them. (c) Composite fabricated at a curing pressure of 0.5 MPa, showing a single lamina and parts of two laminae adjacent to it. [10].

crossply [0/90] continuous carbon fiber epoxy-matrix composite. In Fig. 3(a) and 3(b), parts of only two of the laminae are shown, with the bottom lamina having fibers perpendicular to the plane of the page, whereas the top lamina have fibers in the plane of the page. The interlaminar interface is relatively rich in the polymer matrix, with an interface thickness typically ranging from 3 to 10 μm (Table 2, Fig. 3(a)). This thickness is smaller when the curing pressure is higher (Fig. 3(b)). This is to be distinguished from composites in which the interlaminar interface thickness is chosen to be large (e.g., 20 μm) for the purpose of toughening the composite [11]. Fig. 3(c) shows the structure within a lamina. Some fibers are not exactly parallel to the plane of the polished section, so they appear as if they are not continuous.

3.2. Woven fabrics

Woven fiber fabrics involve differently oriented fiber tows that are woven together. The number of fibers in a tow typically ranges from 3000 (known as 3 K) to 60,000 (known as 60 K) and the cross-sectional shape of a tow is typically circular. Their handling is easier than that of unidirectional fibers. However, the weaving necessarily involves the bending of the fibers (Fig. 4). As a result, the fiber bending degrades the mechanical properties of the composite. The use of tows that are ribbon-like rather than circular in cross-section alleviates this problem, in addition to allowing the fabric to be less porous.

4. Processing-structure-property relationships

The processing-structure-property relationships are organized and presented in this section in terms of how specific processing/structure parameters affect various properties. The processing/structure parameters include the fiber lay-up, fiber weaving configuration, fiber type, fiber treatment, curing pressure, fiber volume fraction, fillers and their distribution and volume fraction, nanofibers grown on the carbon fibers, interlayers between the fiber laminae, z-pinning in the through-thickness direction, and coating of the composite. The properties relate to the property anisotropy, static/dynamic mechanical properties, viscoelastic behavior, toughness, fatigue resistance, wear resistance, ablation resistance, fire resistance, environmental resistance, temperature effects, polymer matrix glass transition effects, polymer matrix melting effects, humidity effects, thermal conductivity, thermal expansion, dielectric behavior, electric permittivity, electrical conductivity, electromagnetic interference (EMI) shielding, thermoelectric behavior, electrical-resistance-based self-sensing, self-healing ability, and the condition of the interface between contacting unbonded composites (relevant to fastened joints).

4.1. Unidirectional vs. composite and woven fabric composite

Table 3 compares the mechanical properties of unidirectional and fabric carbon fiber epoxy-matrix composites that involve the same type of carbon fiber and the same type of epoxy resin. First, consider the properties of the unidirectional composite. The tensile modulus in the 0° direction (the longitudinal direction) is much higher than that in the 90° direction (the transverse direction), as expected. The in-plane shear modulus is even lower than the 90° tensile modulus, indicating the weakness of the interlaminar interface. The ultimate tensile strength and the ultimate compressive strength are much higher in the 0° direction than the 90° direction, as expected. The 0° tensile strength is higher

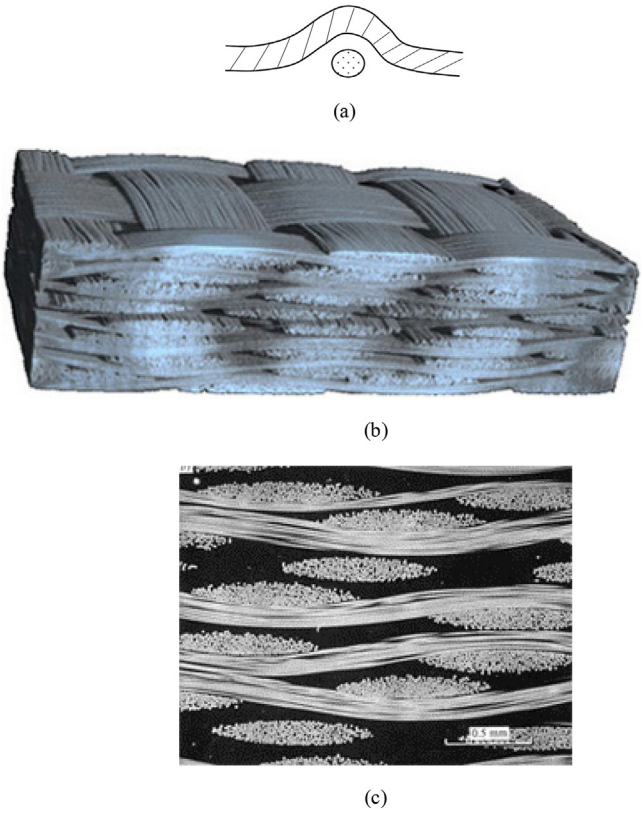

Fig. 4. (a) The bending of one fiber over another due to weaving. (b-c) A woven continuous fiber polymer-matrix composite. (b) A three-dimensional view. (c) A cross-sectional view showing the fabric layers, with each layer consisting for fibers oriented in the plane of the page and in the direction perpendicular to the page. (b-c) (http://www.composites.ugent.be/home_made_composites/what_are_composites.html, public domain).

than the 0° compressive strength, due to the superior strength of the fiber under tension than compression. However, the 90° tensile strength is lower than the 90° compressive strength, due to the dominance of the polymer matrix in governing the 90° behavior. The in-plane shear strength is low, though it is higher than the 90° tensile strength. The 0° ultimate tensile strain (ductility) is higher than the 0° ultimate compressive strain, due to the dominance of the fibers in governing the 0° behavior, but the 90° ultimate tensile strain is lower than the 90° ultimate compressive strain, due to the dominance of the polymer matrix in governing the 90° behavior. The 0° ultimate tensile strain is higher than the 90° ultimate tensile strain, due to the much higher tensile strength in the 0° direction. However, the 0° ultimate compressive strain is lower than the 90° ultimate compressive strain, due to the dominance of the fibers in governing the 0° behavior and the dominance of the polymer matrix in governing the 90° behavior. The ultimate in-plane shear strain is quite high, though it is lower than the 90° ultimate compressive strain. The CTE is negative and close to zero in the 0° direction, but is positive and much greater in magnitude in the 90° direction, again due to the dominance of the fibers in governing the 0° behavior and the dominance of the polymer matrix in governing the 90° behavior. The composite density (1.60 g/cm^3) is lower than that of the fiber itself (1.76 g/cm^3 for the PAN-based T300 fiber), due to the presence of the polymer matrix in the composite.

Table 3
Mechanical properties of continuous carbon fiber epoxy-matrix composites (120 °C curing), with comparison of unidirectional (0°) composite and fabric composite, both involving a standard-modulus fiber (Toray T300).

Property	0°, 60 vol.%	Fabric, 50 vol.%
Tensile modulus, 0°	135 GPa	70 GPa
Tensile modulus, 90°	10 GPa	70 GPa
In-plane shear modulus	5 GPa	5 GPa
Major Poisson's ratio	0.30	0.10
Ultimate tensile strength, 0°	1500 MPa	600 MPa
Ultimate compressive strength, 0°	1200 MPa	570 MPa
Ultimate tensile strength, 90°	50 MPa	600 MPa
Ultimate compressive strength, 90°	250 MPa	570 MPa
Ultimate in-plane shear strength	70 MPa	90 MPa
Ultimate tensile strain, 0°	1.05%	0.85%
Ultimate compressive strain, 0°	0.85%	0.80%
Ultimate tensile strain, 90°	0.50%	0.85%
Ultimate compressive strain, 90°	2.50%	0.80%
Ultimate in-plane shear strain	1.40%	1.80%
CTE, 0°	-0.30×10^{-6}/K	3.20×10^{-6}/K
CTE, 90°	28.00×10^{-6}/K	2.10×10^{-6}/K
Density	1.60 g/cm^3	1.60 g/cm^3

http://www.performance-composites.com/carbonfibre/mechanicalproperties_2.asp.

Comparison between the 0° composite and the fabric composite shows that the tensile modulus is the same in both 0° and 90° directions for the fabric, though they are very different for the 0° composite, as expected, due to the multidirectional configuration of the fibers in the fabric composite. The major Poisson's ratio is lower for the fabric composite than then 0° composite, due to the multidirectional configuration of the fibers in the fabric restraining the transverse shrinkage that is associated with the Poisson effect. The 0° tensile/compressive strength is lower for the fabric composite than the 0° composite, whereas the 90° tensile/compressive strength is higher for the fabric composite than the 0° composite, as expected. The ultimate in-plane shear strength is higher for the fabric composite than the 0° composite, because of the greater degree of waviness of the fibers in the former. The 0° ultimate tensile strain is lower for the fabric composite than the 0° composite, but the 90° ultimate tensile strain is higher for the fabric composite than the 0° composite; these differences in ultimate strain reflect the abovementioned differences in the tensile strength. The 0° ultimate compressive strain is slightly lower for the fabric composite than the 0° composite, due to the slight restraint imposed by the multidirectionality of the fibers in the fabric. However, the 90° ultimate compressive strain is much lower for the fabric composite than the 0° composite, because of the dominance of the matrix in governing the transverse behavior of the 0° composite. The ultimate in-plane shear strain is higher for the fabric composite than the 0° composite, because of the higher ultimate in-plane shear strength for the fabric composite.

For a unidirectional composite with PAN-based carbon fiber (HexTow IM7, with CTE = -0.64×10^{-6}/°C) and an epoxy matrix (CYCOM 977-2 toughened epoxy system, with CTE = 56×10^{-6}/°C), the CTE is -0.76×10^{-6}/°C (close to the fiber value), 36.3×10^{-6}/°C and 36.0×10^{-6}/°C in the longitudinal, transverse and through-thickness directions, respectively. For a composite with the same fibers (but woven with the plain weave rather than being unidirectional) and matrix, the CTE is 4.02×10^{-6}/°C, 3.22×10^{-6}/°C and 56.5×10^{-6}/°C in the longitudinal, transverse and through-thickness directions, respectively. For both unidirectional and woven fiber composites, the through-thickness CTE is dominated by the matrix. The CTE value of the woven fiber composite (56.5×10^{-6}/°C) is close to that of the matrix material (56×10^{-6}/°C). The CTE value is lower for the unidirectional composite (36.0×10^{-6}/°C) than the woven fiber composite (56.5×10^{-6}/°C), probably because of the greater thickness of the interlaminar interface for the woven composite (~3-mm thick 16-lamina laminate) than the unidirectional composite (32-lamina ~3-mm thick laminate). For the unidirectional composite, the transverse CTE is essentially equal to the through-thickness CTE, indicating that the thermal expansion is dominated by the matrix for both transverse and through-thickness directions. In contrast,

for the woven fiber composite, the CTE is similar for the longitudinal and transverse directions; this is expected, due to the 90°-biaxial configuration of the weaving causing the presence of fibers along both directions. [12]

4.2. Longitudinal vs. transverse properties of a unidirectional composite

Fig. 5 shows flexural stress-strain curves for a unidirectional carbon fiber epoxy-matrix composite in the 0° and 90° directions. For both directions, the curve is a straight line up to failure, indicating the elastic nature of the deformation and the essential absence of plastic deformation prior to failure. The modulus values are 214 ± 6 and 7.5 ± 1.0 GPa in the 0° and 90° directions, respectively, and the strength values are 1561 ± 30 and 59 ± 3 MPa in the 0° and 90° directions, respectively [13]. This difference in the 0° and 90° flexural behavior is consistent with the difference in the 0° and 90° tensile behavior described in Table 3 and is in contrast to the difference in the 0° and 90° compressive behavior described in Table 3. This implies that the flexural properties (both modulus and strength) relate to the tensile properties (both modulus and strength) rather than the compressive properties. Even though a beam under flexure experiences tension on one surface and compression on the opposite surface, it is the deformation on the tension surface that governs the flexural behavior.

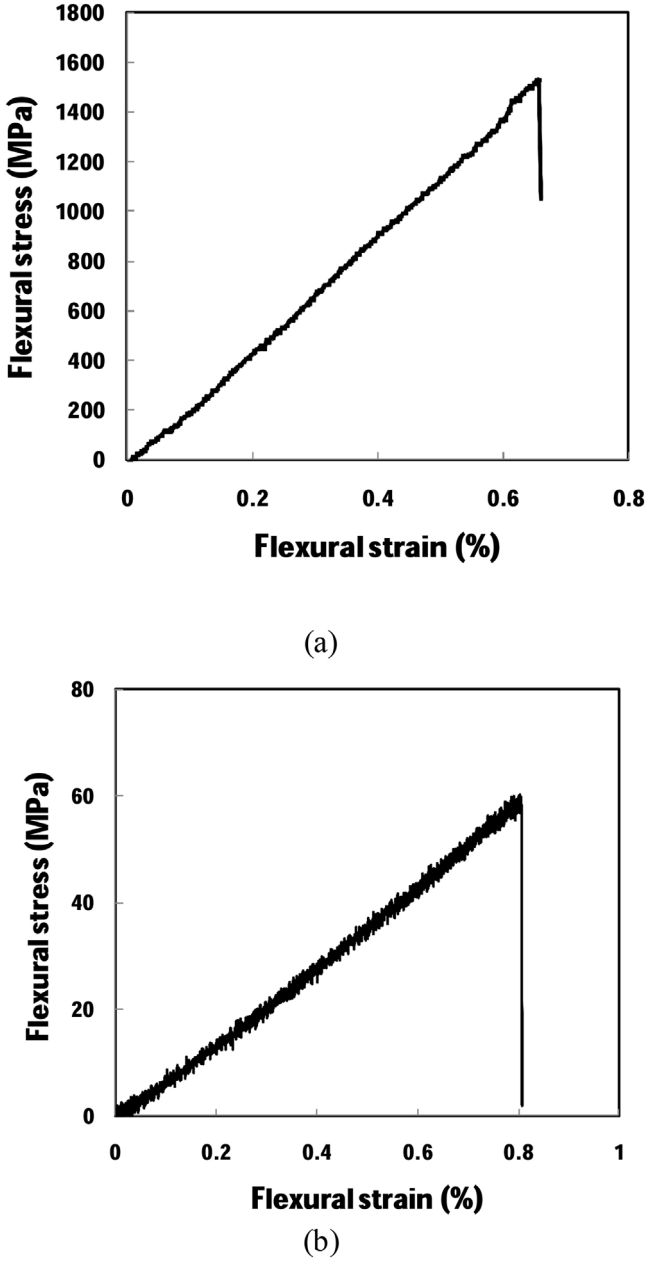

Fig. 5. Curves of flexural stress versus flexural strain during static flexure up to failure for the unidirectional carbon fiber epoxy-matrix composites (0.5 MPa curing pressure). (a) 0° composite. (b) 90° composite. [13].

4.3. Effects of the curing pressure and fiber lay-up configuration

The curing pressure and fiber lay-up configuration affect the static and dynamic mechanical properties, fatigue resistance and through-thickness thermal conductivity, as described below.

4.3.1. Static mechanical properties

Table 4 shows that the flexural strength and modulus are increased by increasing the curing pressure from 0.5 to 2.0 MPa, while the ductility is decreased, whether the fiber lay-up configuration is crossply or unidirectional. For the same curing pressure (whether 0.5 or 2.0 MPa), the unidirectional composite gives higher strength and modulus, but lower ductility. These effects of the curing pressure are consistent with the effect of the curing pressure on the fiber volume fraction (Table 1).

Table 4 shows the measured and calculated values of the static flexural modulus of each composite. The calculation is based on the Rule of Mixtures for the modulus.

4.3.2. Fatigue resistance

Carbon fiber polymer-matrix composites are excellent in the fatigue resistance compared to metals, wood epoxy laminate and glass fiber polymer-matrix composites for fatigue life exceeding about 100,000 cycles. At a stress amplitude equal to 50% of the strength, the fatigue life is essentially infinity. The failure modes of the composites are complex, with fatigue damage involving a combination of matrix cracking, longitudinal splitting, fiber fracture and delamination [14].

The fatigue resistance of a composite structure depends on the fiber lay-up configuration. This is because the viscoelastic behavior of the polymer matrix affects the fatigue life and the degree of contribution of the matrix depends on the fiber lay-up configuration [15].

4.3.3. Dynamic mechanical properties

Table 5 shows that, for the same curing pressure of 2.0 MPa and longitudinal flexural loading, the unidirectional composite gives lower loss tangent and higher storage modulus. This is expected, since the longitudinal behavior is dominated by the fibers and the longitudinal fiber content is greater for the unidirectional composite than the crossply composite. Table 5 also shows that, for the unidirectional composite and the same curing pressure of 2.0 MPa, the transverse flexural loading gives greater loss tangent and lower storage modulus than the longitudinal flexural loading, as expected, since the matrix contributes much more to the transverse behavior than the longitudinal behavior. Furthermore, Table 5 shows that, whether the composite is crossply or unidirectional, an increase in curing pressure from 0.5 to 2.0 MPa decreases the loss tangent and increases the storage modulus. The energy dissipation ability, which relates to the loss modulus, is higher for the unidirectional composite than the crossply composite, whether the curing pressure is 0.5 or 2.0 MPa; this reflects the higher storage modulus for the unidirectional composite than the crossply composite.

The viscoelastic properties described in Tables 5 are all for room temperature. This behavior is to be distinguished from the

Table 4
Effects of lay-up configuration and curing pressure on the static flexural strength, modulus and ductility (strain at failure) of continuous carbon fiber epoxy-matrix composites. [10].

Lay-up configuration	Curing pressure (MPa)	Measured strength (MPa)	Measured modulus (GPa)	Calculated modulus (GPa)[a]	Measured ductility (%)
Crossply	0.5	789 ± 17	123 ± 2	124	0.850 ± 0.054
Crossply	2.0	1008 ± 24	147 ± 4	148	0.648 ± 0.030
Unidirectional	0.5	1561 ± 30	214 ± 6	215	0.708 ± 0.034
Unidirectional	2.0	1579 ± 167	252 ± 4	253	0.621 ± 0.061

[a] Based on the Rule of Mixtures.

Table 5
Dynamic flexural properties (three-point bending, 0.2 Hz, sinusoidal, room temperature) of continuous carbon fiber epoxy-matrix composites. [10].

	Loss tangent	Storage modulus (GPa)	Loss modulus (GPa)
Crossply, 0.5 MP, longitudinal	0.0086 ± 0.0002	126 ± 2	1.10 ± 0.04
Crossply, 2.0 MPa, longitudinal	0.0079 ± 0.0001	161 ± 8	1.28 ± 0.06
Unidirectional, 0.5 MPa, longitudinal	0.0080 ± 0.0001	199 ± 16	1.61 ± 0.12
Unidirectional, 2.0 MPa, longitudinal	0.0067 ± 0.0004	251 ± 8	1.69 ± 0.11
Unidirectional, 2.0 MPa, transverse	0.0092 ± 0.0007	11 ± 1	0.10 ± 0.01

behavior around the glass transition temperature (T_g) of the polymer matrix. Around the glass transition temperature, the storage modulus decreases and the loss tangent exhibits a peak [16].

4.3.4. Through-thickness thermal conductivity

A higher curing pressure tends to result in a smaller thickness of the interlaminar interface region of the resulting composite, as this region is relatively rich in the matrix. This in turn enhances the thermal conductivity of the composite in the through-thickness direction [17].

Due to the structure of a carbon fiber polymer-matrix composite laminate, a number of quantities are expected to contribute to the through-thickness thermal conductivity of the laminate. These quantities include the thermal resistivity within a lamina and that of the interlaminar interface. In particular, the thermal resistivity within a lamina consists of that of the fibers in the lamina and that of the fiber–fiber interfaces in the lamina.

The thermal resistivity (with unit m^2.K/W) is independent of the area; the thermal resistance (with unit K/W) depends on the area. If there are N laminae, there are N-1 interlaminar interfaces and the through-thickness thermal resistivity R of the composite is given by

$$R = N\,R_\ell + (N-1)\,R_i, \quad (1)$$

where R_ℓ is the through-thickness thermal resistivity of a lamina and R_i is that of an interlaminar interface. The R_ℓ and R_i, may be determined by measuring R for different values of N. [17]

Fig. 6 shows the plot of through-thickness thermal resistivity vs. thickness for the composite containing carbon black (CB), fabricated at 0.1 MPa. That the plot is a straight line means that $R = NR_\ell$ and R_i is essentially 0. The slope of this line is the inverse of the thermal conductivity. The intercept with the vertical axis at zero thickness is the thermal resistivity of the two specimen-contact interfaces. The contact refers to the thermal contact, which, in this case, is copper. The resistivity of a specimen-copper interface ranges from 6×10^{-5} to 1×10^{-4} m^2.K/W. The lamina resistivity R_ℓ is obtained by dividing the composite resistivity (with the specimen-copper resistivity excluded) by N. [17]

The through-thickness thermal resistivity of a lamina is given by

$$R_\ell = R_f + R_j, \quad (2)$$

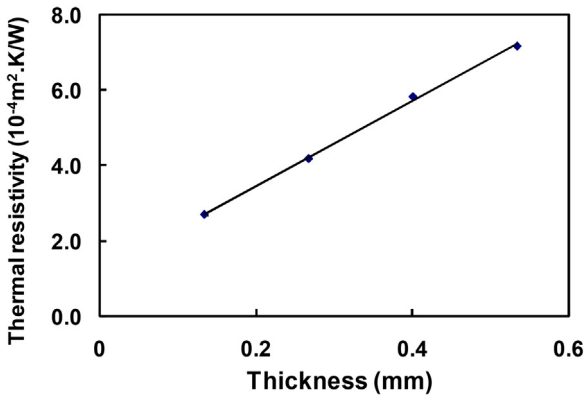

Fig. 6. Plot of thermal resistivity vs. thickness for the composite containing carbon black (CB), fabricated at a curing pressure of 0.1 MPa [17].

where R_f is the thermal resistivity of all of the M (26, from microscopy) fibers stacked along the thickness of the lamina and is related to the transverse thermal conductivity κ_f (7 W/m.K) of a single fiber of diameter d (7 μm) by

$$R_f = Md/\kappa_f = 2.6\times10^{-5}\ m^2.K/W \quad (3)$$

and R_j is the thermal resistivity of all the interfaces between the stacked fibers in the lamina (i.e., the intralaminar fiber–fiber interfacial thermal resistivity). As shown in Table 5, R_ℓ is dominated by R_j. Even if the value of κ_f is lower than the assumed value of 7 W/(m.K) (due to the fiber anisotropy), R_j amounts to a substantial fraction of R_ℓ. The R_f is not expected to change with the curing pressure or the filler, since the structure within a fiber is not affected by the curing pressure or the filler. However, R_j changes (Table 6), since the degree of fiber–fiber contact within a lamina is affected by the curing pressure and can be affected by the filler as well. For example, the filler may affect the degree of waviness of the continuous fibers, which are not perfectly straight anyway.

This finding applies to either curing pressure, with and without filler. Thus, the curing pressure and filler essentially do not affect R_i, which remains negligible, but they affect R_ℓ. Hence, the thermal resistivity is dominated by R_ℓ. A decrease in R_ℓ means that the thermal resistivity associated with the interface (in the form of a number of contact points) between continuous fibers in the same lamina is decreased. [17]

Table 6
Effects of curing pressure (0.1 or 2.0 MPa) and fillers on the thermal conductivity, lamina thermal resistivity R_ℓ and intralaminar fiber–fiber interfacial thermal resistivity R_j [17].

Filler	Conductivity W/(m.K)		R_ℓ (10^{-4} m^2. K/W)		R_j (10^{-4} m^2. K/W)	
	0.1 MPa	2.0 MPa	0.1 MPa	2.0 MPa	0.1 MPa	2.0 MPa
None	0.729	1.091	2.062	1.058	1.80	0.80
Carbon black	0.891	1.212	1.497	0.938	1.24	0.68
K-1100 carbon fiber	0.903	1.444	1.426	0.771	1.17	0.51
SWCNT[a]	0.910	1.453	1.457	0.808	1.20	0.55

[a]Single-walled carbon nanotube

Table 7
Effect of curing pressure on the properties of continuous carbon fiber epoxy-matrix composites in the through-thickness direction. [18,19].

Curing pressure (MPa)	Thermoelectric power (μV/K)	Electrical resistivity (Ω.cm)	Thermal conductivity W/(m.K)	*ZT* at 70 °C
0.5	5.3 ± 0.5	2.95 ± 0.04	1.17 ± 0.02	2.8×10^{-7}
4.0	7.8 ± 1.0	0.171 ± 0.005	1.31 ± 0.01	9.4 x 10^{-6}

Table 7 [18,19] shows that an increase in the curing pressure increases the through-thickness thermoelectric power, decreases the through-thickness electrical resistivity substantially, increases the through-thickness thermal conductivity slightly, and increases the through-thickness *ZT* substantially. These effects are consistent with the decrease in interlaminar interface thickness due to the increase in the curing pressure (Table 2) and the consequent enhanced through-thickness electronic conduction.

4.4. Effects of the direction relative to the fiber direction

Carbon fiber composites are highly anisotropic due to their lamellar structure, with the continuous fibers in the plane of the lamellae. Within a lamina, the fibers are typically all in the same direction. Because a carbon fiber is itself highly anisotropic, with the thermal conductivity much higher in the axial direction than the transverse direction, the thermal conductivity of a lamina is much higher in the fiber direction of the lamina than in the transverse direction. However, for the purpose of obtaining acceptable mechanical properties in all in-plane directions of a composite, a structural composite always involves fibers oriented in different directions for different lamellae. Therefore, the thermal conductivity of a structural composite is high in all in-plane directions, such that the conductivity is limited by the axial thermal conductivity of the fiber. On the other hand, the through-thickness thermal conductivity is much lower than the in-plane conductivity, due to the absence of fibers in the through-thickness direction and the fact that the interface between laminae is relatively rich in the matrix polymer, which is a poor conductor. Thus, the main problem in the thermal conductivity of the composite lies in the through-thickness direction. A similar situation occurs for composites with each lamina in the form of a fabric with woven continuous fibers. However, fabrics are not usually used for high-performance structural composites, because of the bending of the fibers in a fabric.

For a woven carbon fiber epoxy-matrix composite without any filler, the thermal conductivity is 2.0 W/(m.K) in the in-plane direction and 0.32 W/(m.K) in the through-thickness direction [20]. The thermal conductivity of a unidirectional continuous carbon fiber epoxy-matrix composite is 3.6 and 0.74 W/(m;K) at about 30 °C in the longitudinal and transverse directions respectively [22].

The thermal conductivity is the product of the thermal diffusivity, the specific heat and the density. The laser flash method measures the thermal diffusivity. The in-plane thermal diffusivity of a unidirectional continuous pitch-based carbon fiber epoxy-matrix composites decreases as the temperature increases. The ratio of the longitudinal diffusivity to the transverse diffusivity (both in-plane) exceeds 100. [21]

4.5. Effects of the fiber type

The fiber type affects the CTE, thermal conductivity, dielectric properties, EMI shielding effectiveness and thermoelectric power, as described below.

4.5.1. Thermal expansion

The CTE of a continuous carbon fiber composite lamina is anisotropic, because of (i) the alignment of the carbon fibers, (ii) the low CTE of the fibers compared to the polymer matrix, and (iii) the difference in CTE between the axial and transverse directions of a fiber. The anisotropy can result in warpage of the composite laminate. The use of a quasi-isotropic lay-up configuration of the fibers in the different laminae of a composite (Fig. 2(a)) alleviates this problem. Improvement the bond between the carbon fiber and a polyamide matrix by using a coupling agent reduces the CTE of the composite [23].

The in-plane CTE of a continuous carbon fiber epoxy-matrix composite is governed by the fiber type. The value is -1×10^{-6}/°C (negative) in case of a pitch-based carbon fiber, 0.4×10^{-6}/°C in case of an ultrahigh modulus PAN-based carbon fiber, and 2.3×10^{-6}/°C in case of an intermediate modulus PAN-based carbon fiber [24].

4.5.2. Thermal conductivity

The in-plane thermal conductivity of a continuous carbon fiber composite is governed by the carbon fiber type. Pitch-based carbon fiber gives higher thermal conductivity than PAN-based carbon fiber. For example, an epoxy-matrix composite with continuous pitch-based carbon fiber exhibits in-plane thermal conductivity 330 W/(m.K), whereas the epoxy-matrix composite with continuous PAN-based carbon fiber exhibits in-plane thermal conductivity 23 W/(m.K) for the case of an ultrahigh modulus PAN-based fiber and 6 W/(m.K) for the case of an intermediate modulus PAN-based fiber [24].

Although the through-thickness thermal conductivity of a continuous carbon fiber polymer-matrix composite is governed by the matrix, it is affected by the type of carbon fiber. For example, the through-thickness thermal conductivity of a continuous carbon fiber epoxy-matrix composite is 3–10 W/(m.K) for the case

of a pitch-based fiber, and is 0.5 W/(m.K) for the case of a PAN-based fiber (whether intermediate modulus fiber or ultrahigh modulus fiber) [24].

4.5.3. Dielectric behavior

The dielectric behavior is mainly described by the relative dielectric constant (i.e., the relative permittivity, or the real part of the complex relative permittivity). Electric polarization refers to the separation of the positive and negative charge centers in a material, which is said to be a dielectric material. The extent of polarization increases with the electric field in the material. Electric permittivity refers to the extent of polarization per unit electric field. Unless stated otherwise, the relative permittivity refers to the real part of the complex permittivity. The complex relative permittivity ε is expressed as

$$\varepsilon = \varepsilon' + i\,\varepsilon'', \quad (4)$$

where ε' is the real part and ε'' is the imaginary part. The imaginary part exists due to the dielectric loss, which is particularly high when the material is conductive to a degree. The ratio $\varepsilon''/\varepsilon'$ is equal to tan δ, which is known as the loss tangent or the dielectric loss factor.

A high magnitude of the permittivity is attractive for capacitors, which provide electrical energy storage. Energy storage is needed for electric vehicles and self-powered structures. A conventional capacitor is in the form of a dielectric material sandwiched by electrically conductive Plates – a configuration known as a parallel-plate capacitor. This type of capacitor is known as a dielectric capacitor, which is to be distinguished from a super-capacitor (i.e., an electric double-layer capacitor, also known as an ultracapacitor).

For continuous carbon fiber (triangular cross section, with dimension ~8 μm on each side of the triangle, 46 vol.% fiber, unidirectional) in epoxy, ε' at 8.2 GHz is 3.5 when the electric field is parallel to the fibers and is 110 when the electric field is transverse to the fiber direction, and ε'' at 8.2 GHz is 11 and 10 for the parallel and transverse directions, respectively. The triangular shape is supposed to enhance the microwave absorption, though no comparison with other shapes was provided. The numerous fiber-matrix interfaces in the transverse direction probably contribute to causing the relatively high value of ε' in this direction [25].

4.5.4. Electromagnetic interference shielding

Electromagnetic radiation is associated with both an electric field and a magnetic field. These fields can interact with a material, thus causing the radiation to be absorbed and/or reflected by the material. Electromagnetic interference (EMI) shielding refers to the blocking of radio waves, so that they cannot interfere electronic devices [26]. The mechanisms include both absorption and reflection of the radiation. Due to the electrical conductivity of carbon fibers and the ability of the carbon to absorb and reflect electromagnetic radiation, carbon fiber composites are used for EMI shielding, which is needed to protect electronics from interference from radio waves such as those emitted from cellular phones and microwave devices and to prevent the radiation to be emitted from the sources [26–28].

The use of activated carbon fibers with specific surface area 90 m^2/g as a continuous reinforcement (35 vol.%) in a polymer–matrix composite enhances the EMI shielding effectiveness of the composite, due to multiple reflections. The shielding effectiveness at 1.0–1.5 GHz is 39 dB, compared to a value of 30 dB when untreated fibers are used. The activation treatment does not degrade the tensile properties of the fibers, due to the mild degree of the activation [29].

4.5.5. Thermoelectric power

Due to the need for renewable energy to alleviate the energy crisis, thermoelectric energy generation, which refers to the conversion of thermal energy (such as waste heat) to electrical energy, is of great current importance in both science and technology. The development of thermoelectric materials has focused on various alloys and compounds, particularly semiconductors and ceramics [30–32] that have been designed with the goal of attaining the combination of high thermoelectric power, low thermal conductivity and high electrical conductivity, as needed for efficiency in the energy conversion.

The thermoelectric power of a continuous carbon fiber epoxy-matrix composite in the longitudinal direction is low, due to the inherently low value for the carbon fiber. The thermoelectric power can be positive or negative, depending on the type of carbon fiber.

In case that the carbon fiber is relatively graphitic (e.g., Thornel P-100 mesophase-pitch-based carbon fiber), the fiber can be intercalated (with the intercalate between the carbon layers), thereby increasing both the electrical conductivity and the thermoelectric power. By using an intercalate that is an electron acceptor (e.g., bromine), the fiber becomes p-type (not a semiconductor, but a hole metal), so that the thermoelectric power of the carbon fiber epoxy-matrix composite in the longitudinal direction is changed from −4 (negative) to +41 (positive) μV/K. By using an intercalate that is an electron donor (e.g., sodium), the fiber becomes n-type (not a semiconductor, but an electron metal), so that the thermoelectric power of the carbon fiber composite in the longitudinal direction is changed from −4 to −50 μV/K. By stacking dissimilar fiber laminae in a laminate, the interlaminar interface becomes a thermocouple junction. Thermocouple sensitivity up to 82 μV/K has been achieved [33].

4.6. Effects of the fiber volume fraction

An increase in the fiber volume fraction enhances the mechanical properties of the composite, though an excessively high fiber volume fraction causes the properties to be reduced from the maximum values, due to inadequate binding of the fibers by the polymer matrix. In case of epoxy as the matrix, it has been shown that the flexural properties are enhanced as the fiber volume fraction is increased from 50 to 70 vol.%, but are reduced when the fiber volume fraction is further increased to 80 vol.% [34]. In a conventional structural composite, the continuous fiber volume fraction is high (e.g., 60%) and does not vary significantly.

The flammability and combustibility of carbon fiber epoxy-matrix composites decrease with increasing fiber volume fraction. However, the yield of the main gaseous products (such as NO, CO, CO_2, HCN, H_2O, and lightweight hydrocarbons) and the oxygen consumption during the thermal decomposition of the composite increase slightly with increasing fiber volume fraction. Furthermore, a small increase of the fiber volume fraction results in sharp decreases of the heat release rate and the total heat release [35].

Due to the high toughness of the polymer matrix compared to the carbon fiber, the impact strength of continuous carbon fiber polymer-matrix composites decreases with increasing fiber volume fraction. The impact strength of the composite also decreases with decreasing temperature, due to the decreasing toughness of the polymer matrix as the temperature decreases [36]. Fracture mainly involves delamination, though fiber splitting and matrix cracking also occur.

A primary application of the viscous behavior of materials is vibration damping. The damping is known as passive damping, because it exploits the inherent damping ability of materials and

does not involve devices such as sensors and actuators. In passive damping, the mechanical energy is consumed, due to its being converted to another form of energy, typically heat. For solid materials, δ can exceed 0°, but is much less than 90°. Such solids are said to be viscoelastic.

The storage modulus is the dynamic elastic modulus, which is associated with the stiffness. The loss modulus E'' is the dynamic viscous modulus, which relates to the energy loss per unit volume. In accordance with rheology [37], these quantities are described by the following equations:

$$E' = \frac{\sigma_0}{\varepsilon_0}\cos\delta, \tag{5}$$

where σ_0 is dynamic stress amplitude and ε_0 is dynamic strain amplitude (Fig. 7),

$$E'' = \frac{\sigma_0}{\varepsilon_0}\sin\delta, \tag{6}$$

and

$$\tan\delta == \frac{E''}{E'}. \tag{7}$$

The curve of stress vs. strain in a cycle of loading and unloading that spans positive and negative values of the stress is illustrated in Fig. 7 for a viscoelastic material with a nonzero value of δ. The area enclosed by the hysteretic curve is the energy loss per cycle per unit volume.

The ellipse in Fig. 7 can be represented by the equation

$$\left(\frac{\sigma}{\sigma_0}\right)^2 + \left(\frac{\varepsilon}{\varepsilon_0}\right)^2 = (\sin\delta)^2 + 2\left(\frac{\sigma}{\sigma_0}\right)\left(\frac{\varepsilon}{\varepsilon_0}\right)\cos\delta, \tag{8}$$

which is the equation of an ellipse with the principle axis inclined to the abscissa by the angle δ. The area of the ellipse is given by [37]

$$A = \pi\sigma_0\varepsilon_0\sin\delta. \tag{9}$$

Substituting Eq. (6) into Eq. (9) gives

$$A = \pi{\varepsilon_0}^2 E''. \tag{10}$$

In case that the time variation is sinusoidal, the time-varying stress σ and strain ε with the angular frequency ω (with $\omega = 2\pi f$, where f is the frequency) can be expressed by the equations

$$\sigma = \sigma_s + \sigma_0\sin(\omega t), \tag{11}$$

and

$$\varepsilon = \varepsilon_s + \varepsilon_0\sin(\omega t - \delta), \tag{12}$$

where σ_s and ε_s are the static stress and static strain respectively, and σ_o and ε_o are the dynamic stress and dynamic strain respectively. The strain wave lags the stress wave by the phase angle δ. The loss energy per unit volume given by Eq. (9) can be verified by numerical calculation using Eq. (10), in case that the time variation is sinusoidal.

As shown in Table 1, an increase in the fiber volume fraction enhances the storage modulus (i.e., increasing the elastic character) and the loss modulus (i.e., the energy dissipation), but decreases the loss tangent (i.e., decreasing the viscous character). This is expected, since the fibers are responsible for the elastic character, while the matrix is responsible for the viscous character. The increase in the loss modulus correlates with the increase in storage modulus.

4.7. Effects of the temperature

The temperature affects the fatigue resistance and viscoelastic behavior, as described below.

4.7.1. Fatigue resistance

The fatigue resistance depends on the temperature. For a composite cylinder made by filament winding of the fibers on a mandrel, the material of the mandrel affects the fatigue life, due to the difference in CTE between the composite and the mandrel. For aluminum as the mandrel material, the fatigue resistance is greater at 85 °C than room temperature and is worse at −40 °C than room temperature. On the other hand, for a plastic mandrel, the fatigue resistance is worse at 85 °C compared to room temperature [38].

4.7.2. Viscoelastic behavior

The viscous and mechanical-energy-dissipating behavior of materials is needed for vibration damping [39], mechanical energy dissipation (energy loss), mechanical isolation, sound absorption, gasketing and sealing, which are important for the durability, safety, operation and performance of structures and systems. Moreover, vibration reduction and sound absorption are valuable for improving the quality of life of people. This section will not address sound absorption, gasketing or sealing explicitly, but the theory presented may be useful for sound absorption, gasketing and sealing as well, in spite of the difference in frequency between sound and vibrational waves.

The viscous behavior of viscoelastic materials such as rubber and other polymers is well known and is due to the bulk viscous deformation that is enabled by the molecular structure of these materials [40]. However, these materials suffer from their low stiffness (elastic modulus), which results in their ineffectiveness for vibration damping (i.e., mechanical energy dissipation), though they are effective for mechanical isolation by serving as a cushion. Moreover, the viscous character of polymers is strongly dependent on the temperature, with the viscous character being strong only over a narrow temperature range, such as the temperatures around the glass transition temperature. In contrast, ceramics and carbons have much weaker temperature dependence of their viscous behavior. This weak temperature dependence means that the viscous character can be appreciable over a wide range of temperature, including room temperature, which is particularly important for structural applications such as airframe, automobile, wind turbines, helmets, etc.

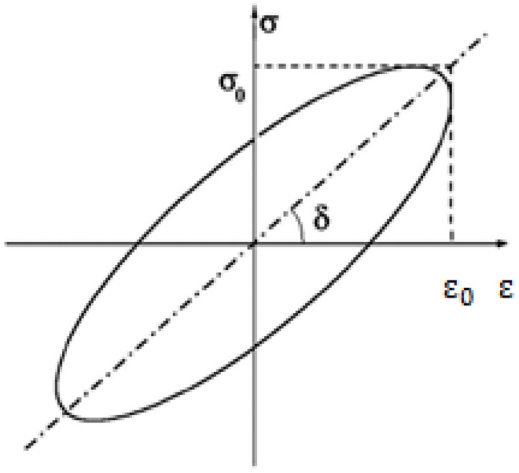

Fig. 7. Graphical representation of the stress-strain relationship of a viscoelastic material with a non-zero value of δ. The σ_0 is the dynamic stress amplitude and is the dynamic strain amplitude. [189].

4.8. Effects of the humidity

In relation to a unidirectional carbon fiber reinforced epoxy that is subjected to reciprocating sliding testing in ambient air at different levels of relative humidity and under full immersion in water, humidity and water immersion affect significantly the fiber debonding. For sliding against stainless steel or alumina, fiber debonding is more significant at low relative humidity than at high relative humidity or under water immersion. The wear depth increases with increasing relative humidity for sliding against stainless steel, but it is essentially independent of the humidity for sliding against alumina. The wear depth is greater when the composite is tested against stainless steel than alumina [41].

4.9. Effects of filler addition

A filler refers to the particles, discontinuous fibers/nanofibers/nanotubes or other discontinuous solid units that are added to a continuous fiber polymer-matrix composite. The filler is present at a volume fraction that is much lower than that of the continuous fibers, which serve as the primary reinforcement. The filler may be distributed in the matrix. Alternatively, the filler is positioned at the interlaminar interfaces, which are regions that are relatively rich in the matrix. The filler addition affects the ablation and fire resistance, static and dynamic mechanical properties, toughness, electrical conductivity, CTE, in-plane and through-thickness thermal conductivity, and through-thickness thermoelectric behavior, as described below.

The addition of a nanofiller to the matrix of a continuous fiber composite is directed at improving certain properties of the composite. The fabrication of a hybrid composite with the nanofiller uniformly distributed throughout the matrix involves the addition of the nanofiller to the matrix precursor and tends to suffer from the increase in viscosity of the matrix precursor and the consequent increasing difficulty of thorough impregnation of the fibers with the matrix precursor [42–45]. With the continuous fibers being in the micrometer scale and the nanofiller being in the nanometer scale, the composite is said to be multi-scale, also said to be hierarchical. Examples of nanoscale fillers are carbon nanotube (CNT) and carbon nanofiber (CNF).

4.9.1. Ablation and fire resistance

Ablation refers to the removal of material from the surface of an object by vaporization, chipping, or other erosive processes. For example, a spacecraft experiences ablation during ascent and atmospheric reentry, due to the high temperatures involved. During ablation conducted using an oxyacetylene torch, a silicone rubber composite filled with silica nanoparticles and short carbon fiber forms a pyrolysis layer, a ceramic layer and a silica layer due to the decomposition, ceramization and oxidation reactions [46].

The addition of alumina nanoparticles (13 nm particle size, from fumed alumina, 5 wt.%) to the epoxy matrix in the fabrication of a continuous carbon fiber fabric epoxy-matrix composite improves the fire resistance slightly. This is attributed to the ability of the alumina nanoparticles to act as a binder for the carbon fibers when the epoxy matrix was burned off at high temperatures [47,48].

4.9.2. Static mechanical properties and fatigue resistance

Rigid particles such as alumina, silica, glass beads, and block copolymers, as well as ceramic whiskers, are used as fillers in carbon fiber epoxy-matrix composites for increasing the strength, stiffness, toughness, and/or fatigue resistance [49,50]. The primary energy-absorbing mechanism for these composites involves a crack-pinning process [50].

The addition of CNT (specifically multi-walled carbon nanotube, abbreviated MWCNT, 0.02 μm diameter, from ILJIN, S. Korea, as prepared by chemical vapor deposition, with purity higher than 95%, the length > 60 μm and average diameter 50 nm) to every interlaminar interface of a crossply carbon fiber epoxy-matrix composite laminate results in a hybrid composite containing 58.6 vol.% continuous carbon fiber, 39.0 vol.% matrix and 2.4 vol.% CNT [13]. The matrix volume fraction is less than the value of 42.1 vol.% for the corresponding unmodified composite (i.e., the composite without CNT), while the fiber volume fraction is slightly higher than the value of 57.9 vol.% for the corresponding unmodified composite. This effect of the CNT on the fiber and matrix volume fractions is due to the method of filler incorporation that involves the application of a solvent-based CNT dispersion (suspension) on the surface of the prepreg (a pre-impregnated sheet of aligned fibers, with each fiber having been coated with the resin). After application of the dispersion, the solvent dissolves away a part of the resin on the surface of the prepreg. Sheets of prepreg are stacked and then consolidated under heat and pressure. The pressure helps both the consolidation of the laminae and the curing of the resin. The curing involves the evolution of gases. The lamina thickness (140 μm), interlaminar interface thickness (8 μm) and composite thickness (2100 μm) are essentially unaffected by the CNT addition. The interlaminar interface region amounts to 5 vol.% of the composite. The short-beam shear strength (53 MPa), i.e., the interlaminar shear strength, is essentially unaffected by the CNT addition.

As shown in Table 8 [13], the flexural modulus of the unmodified and modified composites are 123.0 and 138.0 GPa respectively. This means that the CNT addition enhances the modulus of the composite. Because the continuous fibers are the primary constituent for load bearing, meaningful scientific

Table 8
Flexural modulus/strength/ductility and their fractional change due to the presence of the filler for crossply carbon fiber epoxy-matrix composites fabricated at a curing pressure of 0.5 MPa with and without the interlaminar filler. CNT: multi-walled carbon nanotube; HNT: halloysite nanotube; SiCw: silicon carbide whisker. [13].

Filler content	Modulus (GPa)	Strength (MPa)	Ductility (%)
0	123 ± 2	789 ± 17	0.85 ± 0.05
2.4 vol.% CNT	138 ± 6 (124.5[a])	1002 ± 11 (799[a])	0.73 ± 0.02
1.7 vol.% HNT	141 ± 3 (127.2[a])	958 ± 72 (816[a])	0.67 ± 0.04
1.4 vol.% SiCw	137 ± 3 (126.0[a])	933 ± 51 (808[a])	0.68 ± 0.04
	Fractional change in modulus	Fractional change in strength	Fractional change in ductility
2.4 vol.% CNT	12% ± 6% (11% ± 6%[b])	27% ± 4% (25% ± 5%[b])	−14% ± 8%
1.7 vol.% HNT	15% ± 4% (11% ± 5%[b])	21% ± 12% (17% ± 12%[b])	−21% ± 10%
1.4 vol.% SiCw	11% ± 5% (9% ± 4%[b])	18% ± 9% (15% ± 9%[b])	−20% ± 10%

[a] Calculated value of the unmodified composite, obtained by scaling the measured value of the unmodified composite to the value for the higher fiber volume (Table 4) of the modified composite.
[b] Fractional change relative to the calculated value obtained for the unmodified composite by scaling the measured value of the unmodified composite to the value for the higher fiber volume of the modified composite.

comparison of the unmodified and modified composites should be made at the same continuous fiber volume fraction. Thus, a calculated value (124.5 GPa) of the modulus of the unmodified composite is obtained by scaling the measured value (123.0 GPa) of the unmodified composite to the value for the higher continuous fiber volume of the modified composite. Hence, at the same continuous fiber volume fraction, the CNT addition increases the composite modulus from 124.5 to 138.0 GPa, i.e., an increase of 11%.

Also as shown in Table 8, the flexural strength is increased from 789 to 1002 MPa by the CNT addition. A calculated value (774 MPa) of the strength of the unmodified composite is obtained by scaling the measured value (789 MPa) of the unmodified composite to the value for the higher continuous fiber volume of the modified composite. Hence, at the same continuous fiber volume fraction, the CNT addition increases the composite modulus from 799 to 1002 MPa, i.e., an increase of 25%.

Although both the modulus and strength are increased by the CNT addition, the ductility is decreased by 14%, as shown in Table 8. The fractional decrease in ductility, the fractional increase in modulus and the fractional increase in strength due to the CNT addition are comparable to the corresponding values for halloysite nanotube (HNT, low-cost natural aluminosilicate clay nanotubes with outer diameter 0.1 μm) addition and for silicon carbide whisker (SiC_w, with diameter 1 μm) addition. However, among the three types of filler, SiC_w is the least effective, as it gives the lowest fractional increase in strength; this probably relates to the large diameter of SiC_w. The effectiveness is similar for CNT and HNT. The latter is much less expensive than the former.

The incorporation of carbon nanofibers (CNFs) in a woven continuous carbon fiber epoxy-matrix composite is performed by electrospinning PAN nanofibers on the carbon fiber fabric and subsequent stabilization and carbonization of the PAN nanofibers to form CNFs that are attached to the surface of the carbon fiber fabric. The fabric layers are stacked and subjected to vacuum assisted resin transfer molding (VARTM) to form an epoxy-matrix composite. In resin transfer molding (RTM), the infiltration of the matrix or matrix precursor into a mold cavity containing dry continuous fibers is conducted in order to form a composite article with the shape and dimensions that are dictated by the mold [51]. The infiltration can be conducted on a unidirectional fiber preform (i.e., a sheet of aligned continuous fibers held together by widely spaced transverse stitches, [52,53]) or on a woven fabric. The infiltration tends to be easier when the fiber surface is smoother [54]. The amount of CNFs incorporated is controlled by the time of collection of the PAN nanofibers during electrospinning. For a 10-min collection time, the CNF incorporation increases the flexural strength from 380 to 450 MPa, increases the work of fracture from 11 to 16 kJ/m^2, increases the interlaminar shear strength from 25 to 84 MPa, and increases the elastic modulus from 12 to 25 GPa [55].

Neither the incorporation of electrospun PAN nanofibers (0.3–0.4 μm diameter, not CNFs) between the laminae of a continuous carbon fiber epoxy-matrix composite nor the incorporation of silica nanoparticles (mainly ~20 nm diameter) in the epoxy matrix of a continuous carbon fiber composite provides definitively positive effects to the interlaminar fracture behavior of the composite [56].

Continuous carbon fibers are commonly sized for the purpose of improving the ease of handling the fibers during composite fabrication. The sizing is a thin organic coating. Instead of incorporating nanoparticles in the overall matrix, it is possible to incorporate them in the sizing. The incorporation of silica nanoparticles in the epoxy sizing (prepared by the sol-gel method) is used to modify continuous carbon fiber epoxy-matrix composites. The silica addition to the sizing improves the interlaminar shear strength and impact properties. The silica nanoparticles are formed using tetraethoxysilane (abbreviated TEOS, $Si(OC_2H_5)_4$) as the silica precursor, which is mixed with the epoxy resin for the sizing. Above 600 °C, TEOS is converted to silica in accordance with the pyrolysis reaction

$$Si(OC_2H_5)_4 \rightarrow SiO_2 + 2\ (C_2H_5)_2O.$$

The sizing epoxy is modified with 3-isocyanatopropyl triethoxysilane ($C_{10}H_{21}NO_4Si$), which serves as an additional silica precursor. The covalent bond between the epoxy resin and SiO_2 is enabled by the OH group of the epoxy resin reacting with the NCO group of 3-isocyanatopropyl triethoxysilane, which is thereby grafted on the epoxy resin. The mixing involves stirring at 50 °C for 4 h. The SiO_2 content of 5 wt.% in the sizing is optimum. The interlaminar shear strength is increased from 58 MPa for the case of no sizing, to 63 MPa for the case of epoxy sizing without SiO_2, and to 70 MPa for the case of epoxy sizing containing SiO_2. The mechanical work done during crack propagation is increased from 2.17 J for the case of no sizing, to 2.36 J for the case of epoxy sizing without SiO_2, and to 2.67 J for the case of epoxy sizing containing SiO_2 [57].

The incorporation of alumina or stainless steel particles of diameter 40 μm by manual deposition of the epoxy resin with the dispersed particles at the two symmetrically positioned 0°/90° interlaminar interfaces of a continuous carbon fiber $0°_5/90°_2/0°_5$ epoxy-matrix composite laminate increases the flexural strength from 627 to 738 MPa for alumina particles, and to 798 MPa for steel particles, increases the flexural modulus from 39 to 53 GPa for alumina particles and to 71 GPa for steel particles, and increases the fatigue life from 226,000 to 381,000 cycles for alumina particles, and to 1,245,000 cycles for steel particles. The thickness of the modified interlaminar interface is about 100 μm and the thickness of a lamina is about 1000 μm [58]. These thicknesses are about 10 times the corresponding thicknesses of the composites with nanoscale interlaminar fillers, as described in Table 8 [13].

The incorporation of soft particles (silicone rubber particles of size 2 μm) or hard particles (alumina particles of size 30 nm) up to 10 wt.% in the vinyl ester matrix of a continuous woven carbon fiber composite prepared by vacuum-assisted resin transfer molding does not affect the strength or modulus (whether tensile or flexural) of the composite. However, the fracture toughness is affected. The soft particles increase the Mode I interlaminar fracture toughness, but decreases the Mode II interlaminar fracture toughness. The hard particles have little or no effect on the toughness, whether Mode I or Mode II [59].

Ductile tin-lead alloy particles (20–25 pm in size) are effective as a filler in carbon fiber epoxy-matrix composites for increasing their fatigue resistance. These particles are positioned between the carbon fiber prepreg layers and undergo melting during the curing of the epoxy matrix. The melting does not cause the particles to be connected to one another, but enhances the bonding between the particles and the epoxy resin [60]. The origin of the fatigue resistance increase is probably due to the hindrance of the crack propagation from one ply to another by the ductile alloy particles between the plies.

4.9.3. Toughness

Epoxy is brittle among polymers. For increasing the toughness, carboxy-terminated nitrile butadienes (CTBNs) are commonly added to the epoxy resin. These soluble additives phase-separate upon cure and form rubber domains in the epoxy resin. They are known as reactive liquid rubbers. This method of toughening decreases both the modulus and the glass transition temperature. This is because a fraction of the rubber molecules does not participate in the phase separation, but crosslink randomly in the matrix. Moreover, the rubber inclusion increases the viscosity of the resin, thus hindering the infiltration of the resin into a

reinforcement preform. Therefore, the incorporation of nanoparticles in the epoxy resin is another toughening method. The mechanism involving the nanoparticles relates to the slight slippage at the nanoparticle-matrix interface during deformation.

The incorporation of silica nanoparticles in the epoxy resin (with the nanoparticles dispersed by sonication) in the fabrication of a continuous carbon fiber epoxy-matrix composite laminate by resin transfer molding (RTM) toughens the composite. The interlaminar fracture toughness is improved by the nanoparticle incorporation, thereby increasing the delamination resistance. In addition, the Mode I critical energy release rate (*GIC*) is increased by 45%, reaching 437 J/m^2 [61].

The incorporation of both silica nanoparticles and reactive liquid rubber in the epoxy matrix of a continuous carbon fiber composite laminate (nonwoven fibers, with the laminate being fabricated by RTM) toughens the composite. The Mode I critical energy release rate G_{Ic} is increased by the nanoparticle addition from 433 to 621 J/m^2, but the Mode II critical energy release rate G_{IIc} is decreased from 1300 to 1080 J/m^2. The impact resistance is slightly inferior to the rubber-toughened laminate that does not contain the silica nanoparticles. The delaminated area after impact is increased and the compressive strength after impact is decreased by the nanoparticle addition. The inferiority in the impact resistance is probably due to the agglomeration of the silica nanoparticles [62].

4.9.4. Dynamic mechanical properties

The positioning of CNF (0.6 vol.%) between the continuous carbon fiber (7 μm diameter, 56.5 vol.%) laminae in an epoxy-matrix composite greatly increases the degree of viscous character, as shown under flexure for both the transverse and longitudinal directions, in addition to increasing the storage modulus in the transverse direction [63]. Table 9 [10] shows that the CNT incorporation in a carbon fiber epoxy-matrix composite increases the longitudinal loss tangent, but has essentially no effect on the longitudinal storage modulus, as shown under dynamic flexure.

The increase in loss tangent is attributed to the interfacial-friction mechanism of viscous deformation that is made possible by the sliding at the interface between the CNF/CNT and the matrix and that at the interface between adjacent CNFs/CNTs. This mechanism has been modeled analytically [64,65] and is to be distinguished from the conventional mechanism that involves bulk viscous deformation, which is the mechanism exhibited by polymers.

The incorporation of HNT (halloysite nanotube) increases the storage modulus, but has no effect on the loss tangent. This means that HNT is more effective than CNT as a secondary reinforcement in a carbon fiber composite. However, the relatively small aspect ratio of HNT compared to CNT limits the interfacial-friction mechanism of viscous deformation. The energy dissipation ability, which relates to the loss modulus, is highest for the composite with HNT incorporation.

4.9.5. Electrical conductivity

The incorporation of zinc particles (about 5 μm particle size) between the unidirectional continuous carbon fiber prepreg layers in a laminate with 15 vol.% carbon fibers and a phenolic matrix (fabricated by hot pressing without melting the zinc particles) results in monotonic decrease in the resistivity (through-thickness or transverse) with increasing zinc content; the values range from 10^9 Ω.cm in the absence of zinc down to 500 Ω.cm at the highest zinc content. However, the zinc interlaminar filler causes a monotonic decrease of the flexural strength with increasing zinc content, with values ranging from 300 MPa in the absence of zinc down to 170 MPa at the highest zinc content, and a monotonic decrease in the shear strength from 11 MPa in the absence of zinc down to 8.7 MPa at the highest zinc content [66].

The addition of nickel-coated single-walled carbon nanotube (SWCNT, 5–25 nm outer diameter) as a filler to a continuous carbon fiber composite with bismaleimide (BMI) as the matrix is effective for increasing the electrical conductivity. This matrix is attractive for its high-temperature resistance up to 250 °C. The nickel coating enhances the conductivity. The incorporation of this filler in the continuous carbon fiber composite involves spraying on a carbon fiber lamina (without the resin) a dispersion of the filler in a solvent, followed by the infusion of the resin. The spraying method is attractive in that it does not suffer from the issue of the viscosity of the resin being increased by the filler introduction. The alternative method of distributing the filler in the resin, followed by the infiltration of the resin to the fiber preform, is complicated by the increase in viscosity due to the presence of the filler. Because of the absence of the viscosity issue, the spraying method is suitable for the incorporation of a relatively high concentration of the filler. The solvent is ethylene diamine ($C_2H_4(NH_2)_2$). An amine-based solvent is suitable, because nickel (a transition metal) forms a coordination complex with amine groups, which refer to functional groups that contain a nitrogen atom with a lone pair [67].

4.9.6. Electromagnetic interference shielding

The addition of iron nanoparticles to the epoxy resin of a carbon fiber epoxy-matrix composite increases the shielding effectiveness. The reflection loss is increased from 0 to 10.4 dB (16.8 GHz) with the addition of 40 wt.% iron to the epoxy resin [68]. The reflection loss is further enhanced with a gradient distribution of the iron nanoparticles. The distribution is such that the concentration of the nanoparticles is lower near the composite surface at which the electromagnetic radiation is incident. The reflection loss is 26.8 dB (4.9 GHz) when the radiation is incident on this surface, but is 17.9 dB (5.3 GHz) when the radiation is incident on the

Table 9
Effect of filler on the dynamic flexural properties (three-point bending, 0.2 Hz, sinusoidal, room temperature) of crossply continuous carbon fiber epoxy-matrix composites made with a curing pressure of 0.5 MPa. The filler is positioned at all six interlaminar interfaces of the 7-lamina composite. [10].

Property	Filler		
	None	SWCNT[a]	HNT[b]
Composite density (g/cm^3)	1.583 ± 0.005	1.587 ± 0.023	1.624 ± 0.002
Fiber volume fraction	0.579 ± 0.020	0.580 ± 0.002	0.606 ± 0.002
Matrix volume fraction	0.421 ± 0.019	0.400 ± 0.004	0.375 ± 0.005
Filler volume fraction	0	0.020 ± 0.006	0.019 ± 0.005
Loss tangent	0.0086 ± 0.0002	0.0099 ± 0.0004	0.0085 ± 0.0008
Storage modulus (GPa)	127.8 ± 1.7	131.2 ± 7.1	189.9 ± 1.1
Loss modulus (GPa)	1.10 ± 0.04	1.29 ± 0.11	1.61 ± 0.19

[a] Single-walled carbon nanotube.
[b] Halloysite nanotube.

opposite surface (Shah et al., 2016). This effect of the gradient distribution is because a well matched input impedance of the composite to air helps the incident radiation enter the composite and this entrance is necessary for the composite to absorb the radiation. The input impedance is 413 Ω (4.9 GHz) for the surface with a low nanoparticle concentration and is 510 Ω (3.7 GHz) for the surface with a high nanoparticle concentration.

4.9.7. Electrical-resistance-based self-sensing

Continuous carbon fiber polymer-matrix composites are effective for electrical-resistance-based self-sensing of strain and damage [26]. The addition of CNTs to the composite can improve the effectiveness for electrical-resistance-based sensing [69]. However, the improvement is slight, if any, because the continuous carbon fibers dominate the electrical behavior [70].

4.9.8. Thermal expansion

The incorporation of low-CTE ceramic nanoparticles (zirconium tungstate, ZrW_2O_8, 20 vol.% of the resin) in the matrix (cyanate ester) of a continuous carbon fiber polymer-matrix composite decreases the through-thickness CTE (from 81×10^{-6}/°C to 20×10^{-6}/°C) while the in-plane CTE is only slightly affected (decreased from 10×10^{-6}/°C to 2×10^{-6}/°C) [71].

4.9.9. Thermal conductivity

The through-thickness thermal conductivity is increased and R_ℓ and R_j are decreased upon increasing the curing pressure, whether a filler is present or not (Table 10). This effect is because the increase in curing pressure increases the continuous fiber volume fraction and the density, thus decreasing R_j. The fractional increase in through-thickness thermal conductivity and the fractional decreases in R_ℓ and R_j due to the curing pressure increase are lowered by CB and slightly affected by K-1100 or SWCNT.

At 0.1 MPa curing pressure, K-1100 and SWCNT are slightly more effective than carbon black for enhancing the through-thickness thermal conductivity and decreasing R_ℓ and R_j; at 2.0 MPa curing pressure, K-1100 and SWCNT are much more effective than CB (Table 9) [17]. Due to its low cost, carbon black is competitive.

The through-thickness thermal conductivity is increased and R_ℓ and R_j are decreased by any of the fillers, which have negligible effect on the continuous fiber volume fraction. The filler effect is smaller than the curing pressure effect. The effect of the filler on R_j is probably due to a slight increase of the fiber waviness and the consequent increase in the number of contact points between fibers in a lamina. This phenomenon reduces the effect of the curing pressure, because the additional conductive paths between the continuous fibers make the fiber volume fraction and curing pressure less influential [17].

The fractional increase in through-thickness thermal conductivity due to K-1100 short carbon fiber or SWCNT is greater for the higher curing pressure, whereas the fractional increase due to CB is greater for the lower pressure. The fractional increase in through-thickness thermal conductivity and the fractional decreases in R_ℓ and R_j due to a filler are greater for K-1100 or SWCNT than carbon black, such that the difference between carbon black and K-1100 or SWCNT is greater at the higher pressure. Based on R_j, the effect of K-1100 or SWCNT on the lamina microstructure is not affected by increasing the pressure, whereas that of carbon black on the lamina microstructure is reduced by increasing the pressure. Its porous agglomerate structure causes carbon black to be squishable, so that an increase in pressure compacts the carbon black, making it harder for the carbon black to affect the lamina microstructure. The K-1100 and SWCNT are not squishable [17].

The K-1100 and SWCNT are comparably effective for decreasing R_ℓ and R_j (Table 11), and are comparable in the effect of curing pressure (Table 10), in spite of the much smaller size of the latter. This suggests that the ability of a filler to affect the lamina microstructure is not governed by the filler size and supports the absence of filler penetration of the laminae.

For enhancing the through-thickness thermal conductivity, an increase in the curing pressure is recommended. Filler incorporation helps, but by a lesser degree.

The highest value of the through-thickness thermal conductivity obtained by Han and Chung [17] is 1.5 W/m.K. This is lower than the highest value of 3.3 W/m.K reported for carbon fiber polymer-matrix composites containing carbon black as an interlaminar filler (Han et al., 2008) [72]. Han and Chung [17] and Han et al. [72] used the same type of carbon black. The difference in the thermal conductivity is attributed to the difference in the type of prepreg.

The incorporation of 20% boron nitride (BN) particles of size 10 μm as a filler in the resin (matrix precursor) increases the through-thickness thermal conductivity of a carbon fiber fabric composite from 0.45 to 0.75 W/(m.K) [73]. The required conductivity value for spacecraft radiator application is 0.6 W/(m.K).

For the case of a carbon fiber fabric epoxy-matrix composite, the incorporation of CNF (0.1 wt.%) to the matrix results in no change in the in-plane thermal conductivity value of 1.9 W/(m.K), but results in an increase of the through-thickness thermal conductivity at 25 °C from 0.60 to 0.65 W/(m.K) [74]. However, when the CNF is grown on the carbon fibers rather than being mixed with the matrix precursor, the CNF incorporation increases the in-plane thermal conductivity at 25 °C from 1.9 to 2.1 W/(m.K), and increases the through-thickness thermal conductivity at 25 °C from 0.6 to 0.8 W/(m.K) [74]. This means that the CNF incorporation enhances the through-thickness thermal conductivity more than the in-plane thermal conductivity and that the effect is more when the CNF is grown on the fiber rather than being mixed with the matrix precursor. The greater effect of the grown CNF is due to the higher degree of preferred orientation of the grown CNF.

Even for the case of the grown CNF, the highest fractional increase in thermal conductivity is 30% (25 °C), as observed for the through-thickness thermal conductivity. In contrast, the highest fractional increase in through-thickness thermal conductivity reported by Han and Chung [17] is 32–33% (Table 11), as obtained by the incorporation of either short carbon fiber (K-1100, with thermal conductivity 900–1000 W/(m.K)) or SWCNT to the interlaminar interface. Even with the grown CNF, the highest value of the through-thickness thermal conductivity reported by Liang et al. [74] is 0.8 W/(m.K) at 25 °C. This value is lower than the highest value of 1.45 W/(m.K) reported by Han and Chung [17]

Table 10
Fractional changes in through-thickness thermal conductivity, through-thickness lamina thermal resistivity R_ℓ, intralaminar fiber–fiber interfacial thermal resistivity R_j and density due to curing pressure increase from 0.1 to 2.0 MPa [17]. CB = carbon black.

Filler	Conductivity	R_ℓ	R_j	Density
None	50%	−49%	−56%	2.9%
CB	36%	−37%	−45%	3.1%
K-1100	60%	−46%	−56%	3.2%
SWCNT	60%	−45%	−54%	2.9%

Table 11
Fractional changes in thermal conductivity, lamina thermal resistivity R_ℓ and intralaminar fiber–fiber interfacial thermal resistivity R_j due to filler for curing pressures of 0.1 and 2.0 MPa [17]. CB = carbon black.

Filler	Conductivity		R_ℓ		R_j	
	0.1 MPa	2.0 MPa	0.1 MPa	2.0 MPa	0.1 MPa	2.0 MPa
CB	22%	11%	−27%	−11%	−31%	−15%
K-1100	24%	32%	−31%	−27%	−35%	−36%
SWCNT	25%	33%	−29%	−24%	−33%	−31%

Table 12
Composite density and component volume fractions and of carbon fiber epoxy-matrix composites made at a curing pressure of 4.0 MPa [18,19]. CB = carbon black.

ZT	Composite density (g/cm^3)	Interlaminar interface thickness (μm)	Volume fraction					
			Continuous fiber	Matrix	Filler			
					CB	Te	Bi_2Te_3	Total
9.4×10^{-6}	1.650 ± 0.027	2.6 ± 1.5	0.688 ± 0.044	0.312 ± 0.044	0	0	0	0
2.9×10^{-5}	1.664 ± 0.033	2.8 ± 1.7	0.681 ± 0.005	0.286 ± 0.005	0.033 ± 0.002	0	0	0.033 ± 0.002
2.0×10^{-2}	2.160 ± 0.074	17.0 ± 3.8	0.531 ± 0.002	0.308 ± 0.002	0.019 ± 0.001	0.142 ± 0.002	0	0.161 ± 0.003
8.6×10^{-2}	2.236 ± 0.095	18.0 ± 3.6	0.534 ± 0.002	0.305 ± 0.006	0.020 ± 0.001	0.126 ± 0.006	0.016 ± 0.001	0.162 ± 0.008

(Table 11) and much lower than the highest value of 3.3 W/(m.K) reported by Han et al. [72].

The through-thickness thermal conductivity of up to 1.45 W/(m.K) obtained by Han and Chung [17] and up to 3.3 W/(m.K) obtained by Han et al. [71] are both higher than the highest value of 1.2 W/(m.K) reported by Kistner et al. [75] for carbon fiber polymer-matrix composites without composite modification. They are also higher than the highest value of 1.253 W/(m.K) reported by Wrosch et al. [76] for carbon fiber polymer-matrix with copper nanoparticles (25 nm, 14.5 wt.%) and solder network (formed from molten solder particles) at the interlaminar interface. Moreover, they are also higher than the value of 0.7 W/(m.K) reported by Yu et al. [77] without composite modification and the value of 0.86 W/(m.K) reported by Yu et al. [77] for a laminate coated with a highly-oriented graphite film.

4.9.10. Thermoelectric behavior

An effective thermoelectric material needs to have a high thermoelectric power (i.e., Seebeck voltage per unit temperature difference, with the value being positive for positive carriers moving from the hot end to the cold end and being negative for negative carriers moving from the hot end to the cold end), a low electrical resistivity and a low thermal conductivity. The figure of merit (Z) of a thermoelectric material is given by

$$Z = S^2/(\rho k), \tag{13}$$

where S is the thermoelectric power, k is the thermal conductivity, and ρ is the electrical resistivity. The unit of Z is K^{-1}. The dimensionless figure of merit (ZT) of a thermoelectric material is given by the product of Z and the temperature in K, with the temperature being the average temperature in the temperature gradient. The value of ZT relates to the thermodynamic efficiency of the energy conversion [78]. It needs to exceed 2.0 in order to be competitive technologically, but the highest value attained is 1.8 [79].

For a woven carbon fiber epoxy-matrix composite without any filler, the thermoelectric power is 4.0 μV/K in the in-plane direction and 1.8 μV/K in the through-thickness direction. The thermal conductivity is 2.0 W/(m.K) in the in-plane direction and 0.32 W/(m.K) in the through-thickness direction. The electrical resistivity is 6.7×10^{-3} Ω.cm (four-probe method) in the in-plane direction and 176 Ω.cm (two-probe method) in the through-thickness direction; the value in the through-thickness direction is likely an overestimate, due to the two-probe method used. With these values, the dimensionless thermodynamic figure of merit ZT is 2.4×10^{-5} in the in-plane direction and 2.0×10^{-9} in the through-thickness direction. These values are very low [20].

Bismuth telluride (Bi_2Te_3) [80] and tellurium are well-known thermoelectric materials [81,82]. Bismuth telluride is particularly good, with the dimensionless thermoelectric figure of merit ZT about 1. The thermoelectric power of a continuous carbon fiber nylon–matrix structural composite in the through-thickness direction is increased from 0.5 to 22 μV/°C by adding tellurium particles (7.3 vol.%) as an interlaminar filler. The effect of tellurium is negligible in the longitudinal direction than in the through-thickness direction, because the longitudinal behavior is dominated by the carbon fiber [83]. From an application viewpoint, the thermoelectric behavior in the through-thickness direction is important, since the temperature gradient tends to be in the through-thickness direction.

Table 12 shows the density and component volume fractions of the unmodified and modified composites [18,19]. The components are the continuous carbon fiber, the filler(s) and the matrix. The volume fractions of the fiber and matrix are calculated from the measured density, based on the Rule of Mixtures. The volume fraction of a filler is obtained by dividing the volume of the filler by the volume of the composite, with the volume of the filler obtained by dividing the mass of the filler by the density of the filler. The mass of the filler is obtained by subtracting the mass of the prepreg (3.0 × 3.0 cm) that has been treated by the solvent without the introduction of this filler (either as the sole filler or an additional filler) from the mass of the prepreg that has been treated by the solvent with the introduction of this filler. For example, Bi_2Te_3 is the additional filler relative to the composite that contains carbon black and Te.

The fiber volume fraction is decreased by the presence of tellurium particles, but is essentially not affected by the presence of the carbon black, the volume fraction of which is much lower than that of the tellurium. The composite density is increased by the presence of thermoelectric particles, but is essentially not affected by the presence of the carbon black.

The filler combination corresponding to the composite that exhibits the highest ZT value of 0.086 involves tellurium particles (12.6 vol.% of composite) and bismuth telluride particles (1.6 vol.% of composite) at a volume ratio of 8:1, such that these thermoelectric particles and carbon black (2.0 vol.% of composite) are at a volume ratio of 7:1. This filler combination causes the interlaminar interface thickness to increase from 3 to 18 μm (Table 12) and causes the carbon fiber content to decrease from 69 to 53 vol.%. Since the carbon fiber is the primary reinforcement, this decrease in the fiber content is estimated (based on the Rule of Mixtures) to decrease the elastic modulus of the composite by 23%. Future work should be directed at minimizing the thermoelectric particle volume fraction for the purpose of minimizing the modulus decrease. The lamina thickness is essentially unaffected by the presence of the fillers. The fibers of the adjacent laminae of the composite that exhibits the highest ZT are not in contact.

4.10. Effect of nanofibers grown on the carbon fibers

Nanofibers such as CNTs, CNFs and silicon nitride nanowires grown on carbon fibers enhance the properties such as the electrical conductivity, through-thickness thermal conductivity and mechanical behavior, as described below.

4.10.1. Electrical conductivity

It is possible to grow the CNFs/CNTs on the surface of continuous carbon fibers, thus resulting in a hairy form of carbon

fiber [84,85]. However, composite fabrication involving hairy carbon fibers tends to be difficult, due to the difficulty of packing the fibers close together, as needed to achieve a high volume fraction of continuous fibers in the composite, in addition to the difficulty of handling. Moreover, the difficulty for the matrix or matrix precursor to fill the space between the hairs can cause pores, which are detrimental to the mechanical properties of the composite. Another example of a multi-scale composite is one with silver nanowires [86] grown on the carbon fibers in order to improve the electrical connectivity.

The growth of CNT on conventional carbon fibers and the use of these modified continuous fibers to reinforce epoxy results in an approximately 10% increase in the longitudinal electrical conductivity relative to the corresponding composite without the CNT growth [87]. The conductivity increase is due to (i) the enhanced fiber–fiber contact caused by the CNT and (ii) the contact facilitating current detour from one fiber to another in case that a fiber is defective. More significantly, the CNT growth decreases the through-thickness resistivity from 3×10^4 to 3×10^2 Ω.cm [88], because of the enhanced fiber–fiber contact in the through-thickness direction.

4.10.2. Through-thickness thermal conductivity

The growth of MWCNTs (<5 μm long) on the surface of continuous carbon fibers in a spread 18,000-fiber tow (20 mm wide, ~0.036 mm thick, desized in acetone, and then coated with TEOS, $Si(OC_2H_5)_4$, a SiO_2 precursor) is conducted using ferrocene as the catalyst precursor and xylene as the carbon precursor. Only 8.3% of the fibers in the spread tow are exposed and are thus available for MWCNT growth. Without the spreading, only 2.3% of the fibers are exposed. At the end of the continuous reel-to-reel process, the collection of fibers with grown MWCNT is impregnated with epoxy to form a prepreg, which is known as a MWCNT-studded prepreg tape. The lay-up (crossply configuration) of the prepreg sheets and subsequent consolidation and curing of the stack results in a laminate. The presence of the MWCNTs in the prepreg increases the thermal diffusivity of the laminate in the through-thickness direction from 0.48 to 0.68 mm^2/s, i.e., a 42% increase [89]. If the fractional increase in thermal conductivity is equal to the reported fractional change in thermal diffusivity, the fractional increase in thermal conductivity of 42% is higher than the value of 33% (Table 11 [17]) for the addition of SWCNTs at the interlaminar interface of continuous carbon fiber epoxy-matrix composite.

4.10.3. Mechanical behavior

A carbon fiber fabric may be modified by the growth of silicon nitride (Si_3N_4) nanowires by catalyst-assisted pyrolysis of a ceramic precursor. The nanowires are randomly oriented around the carbon fibers, with diameter 30–150 nm and length of several hundred micrometers. Although the modification is aimed at improving the mechanical properties, results on the mechanical behavior are not available [90].

Similarly, a carbon fiber felt (with short fibers) is modified by the growth of Si_3N_4 nanowires on the felt by catalyst-assisted pyrolysis of polyureasilazane, in which urea provides N and silazane provides Si and N. Polysilazane is a polymer in which silicon and nitrogen atoms alternate to form the backbone of the molecule. Then the modified felt preforms are densified by chemical vapor infiltration (CVI), thereby resulting in carbon–carbon (C/C) composites, i.e., carbon fiber carbon-matrix composites. The composites are attractive in the out-of-plane compressive and interlaminar shear strengths. The mechanical behavior is even better if pyrolytic carbon has been deposited on the carbon fiber surface before the growth of the nanowires [91].

4.11. Effects of interlayers

The interlayer refers to the layer of material positioned between adjacent laminae. It can be a continuous sheet or a discontinuous sheet that allows the polymer matrix to penetrate its pores. The latter is advantageous for promoting the bond between the interlayer and the sandwiching laminae through mechanical interlocking. The interlayers between laminae affect the toughness, viscous behavior, electrical conductivity, wear resistance, self-healing ability, fire resistance, thermal conductivity, CTE and dielectric properties, as described below.

4.11.1. Toughness and viscous behavior

A thin and ductile polymer interlayer (interleaf) is placed between carbon fiber prepreg layers in order to increase (as much as doubling) the toughness of the composite by toughening the interface between the laminae in the laminate. The interleaf is formulated so that it remains a discrete well-bonded void-free layer after it has been cocured with the matrix resin. It may be twenty times thicker than the resin between plies in a conventional laminate. The interleaf also serves to eliminate stress concentrations, which otherwise would produce premature matrix failure [92].

The use of a polymeric interlayer between the laminae of a continuous carbon fiber polymer-matrix composite can be used to increase the fracture toughness [93] and enhance the viscous character [94]. For example, the fracture toughness is increased from 306 to 414 J/m^2 for Mode I and from 718 to 1344 J/m^2 for Mode II [93]. However, this improvement tends to be at the expense of the elastic modulus and strength.

Instead of a polymer interleaf, an aluminum interleaf is used to increase the fatigue resistance of fiber epoxy-matrix composites. In this sandwich composite, an aluminum sheet is placed between adjacent fiber prepreg layers. Aluminum is chosen because of its ductility and low density (for aerospace use). These composites are known as Arall, as well as Fiber Metal Laminates [95].

4.11.2. Electrical conductivity

In case that the interlayer is a porous polymer film that has silver nanowires on its surface, the interlayer can serve to enhance the transverse electrical conductivity. However, the through-thickness conductivity is reduced [93].

4.11.3. Wear resistance

Wear refers to the removal and deformation of material on a solid surface due to the mechanical interaction between solid surfaces. It may involve plastic displacement of the material at the surface and near the surface. In addition, it may involve the detachment of particles, which become the wear debris. For a ductile material such as typical metals, plastic deformation dominates. However, for a brittle material such as a carbon fiber composite, debris formation can become important. A type of wear is known as adhesive wear, which tends to occur between surfaces during frictional contact and typically results in the displacement and attachment of wear debris on a surface. Abrasive wear occurs when hard particles or protuberances are forced against a solid surface and move along the surface. Erosive wear occurs when solid or liquid particles impact a solid surface.

The wear resistance of carbon fiber polymer-matrix composites can be improved by chemical modification of the phenolic binder, electrochemical treatment of the carbon fabric surface, changing the nanostructure of the carbon fibers, and adding a metal particulate filler to the composite [96]. It can also be improved by coating the composite with a nanoparticle filled polymer (e.g., 4 vol.% alumina particle filled epoxy) [97].

4.11.4. Self-healing ability

Self-healing is an attractive function for smart structures. An interlayer in the form of a polymer with a low melting temperature (e.g., 95 °C) may be used for rendering self-healing ability to the carbon fiber composite. The healing requires heating to melt the polymer. The heating can be provided by using the carbon fibers as a heating element [98].

4.11.5. Fire resistance

The addition of an extruded MWCNT-doped polyethersulfone (PES) film as an interlayer positioned between the carbon fiber fabric layers of an epoxy-matrix laminate enhances the flame retardancy relative to the composite without the MWCNTs in the PES film and also relative to the composite without the interlayer. The mechanism for the improvement due to the presence of MWCNTs is probably because the MWCNTs migrate to the composite surface with the melted PES to form a stable char residue [99].

4.11.6. Thermal conductivity and thermal expansion

An aluminum interleaf (interlayer) can be used to increase the thermal conductivity and CTE of fiber epoxy-matrix composites. For use of the composite as a heat sink, the CTE should match as much as possible those of ceramics (e.g., alumina) used in electronic packaging. In this sandwich composite, an aluminum sheet is placed between adjacent fiber prepreg layers. These composites are known as Arall [95]. To achieve a CTE of 6×10^{-6}/°C with a sandwich composite containing aluminum and a Thornel P-100 carbon fiber epoxy-matrix composite, an aluminum content of 45 vol.% is required. The corresponding thermal conductivity is about 189 W/(m.K) [24].

4.11.7. Dielectric behavior

Due to the electrical conductivity of carbon fibers, a continuous carbon fiber polymer-matrix with an electrically insulating matrix can function as a dielectric capacitor, with the carbon fiber laminae serving as the electrically conductive plates of a parallel-plate capacitor. In order for the dielectric loss of the capacitor to be small, the fibers should essentially not make contact across the interlaminar interface. This can be achieved by the incorporation of an electrically insulating layer at the interlaminar interface. The resulting capacitor is known as a structural capacitor, since the composite is a structural material.

Luo and Chung (2001) [100] first reported that a continuous carbon fiber epoxy-matrix composite with writing paper at the interlaminar interface is a dielectric capacitor in the through-thickness direction, with a capacitance of 1.2 μF/m^2 and $\varepsilon' = 5.3$ at 2 MHz This effect was later confirmed by Carlson et al. (2010) and Carlson and Asp (2013), who reported a lower capacitance of 450 nF/m^2 [101,102]. Other workers reported the use of carbon fibers to make supercapacitors [103–105] and batteries [106–109]. A dielectric capacitor requires a dielectric material sandwiched by conductive materials. Compared to supercapacitors and batteries, which require electrodes and electrolytes, dielectric capacitors are attractive for their structural simplicity and high frequency capability. The structural simplicity results in relatively low tendency for the capacitor structure to degrade the mechanical properties of the structural composite. In order to avoid loss in mechanical properties, the fiber volume fraction must remain high. The activation of the fibers, as conducted to increase the fiber surface area [104,105], tends to degrade the mechanical properties of the fibers.

4.12. Effects of fiber treatments

Fiber treatment refers for physical or chemical forms of fiber modification. It can be directed at the surface or bulk of the fiber, but most treatments are directed at the fiber surface, as needed to enhance the bonding of the fibers with the polymer matrix.

The flexural strength and modulus of a continuous carbon fiber polyamide-matrix composite are increased by the treatment of the fiber with a coupling agent. The improvement obtained by using a coupling agent is greater than that obtained by treating the fiber by air oxidation [23].

The sandblasting (using Al_2O_3 particles) of the surface of a continuous carbon fiber epoxy-matrix composite roughens the surface, thereby enhancing the bonding of the composite with a copper coating formed by either electroplating or electroless plating. Due to the polymer matrix on the surface of the composite, the composite is not conductive enough for electroplating, unless it has been pre-treated with palladium [110].

Fiber surface treatment can serve to improve the wetting of the fibers by the resin. The wetting facilitates the penetration of the resin to the space between the adjacent fibers in a tow. Inadequate penetration would result in pores in the resulting composite. Due to the electrical conductivity of carbon fibers, the wettability can be tested by measuring the apparent electrical resistivity of a fiber array during the process of penetration. Due to the non-conductive nature of the resin, the penetration of the resin among the carbon fibers would decrease the degree of contact among the fibers. The decrease in the degree of fiber–fiber contact causes the apparent resistivity of the fiber array in the fiber direction to increase. This is because there is always a degree of damage in some of the fibers and the ability of the electric current to flow from one fiber to an adjacent fiber in case of the presence of a fiber defect allows at least a part of a defective fiber to contribute to electrical conduction. The greater is the wettability, the more is the apparent resistivity increase during the penetration [111,112].

4.13. Effects of the polymer matrix

The polymer matrix is critical, since it serves to bind the fibers together. It affects the elevated temperature, environmental and impact resistance, toughness, matrix glass transition and matrix melting, as described below. Increase of the molecular weight of the thermoplastic polymer matrix improves the impact resistance of the carbon fiber composite, as shown for a polycarbonite (PC) matrix composite [113]. Modification of the thermoplastic matrix can be used to enhance the bond between the carbon fiber and the matrix. For example, maleic anhydride is added to polypropylene (PP) to improve this bond [114].

4.13.1. Elevated temperature resistance

Due to the matrix, the elevated temperature resistance of polymer-matrix composites is limited. In the presence of both heat and humidity (e.g., a hyperthermal environment), an organic matrix may decompose. This may cause delamination in case of a continuous carbon fiber polymer-matrix composite.

4.13.2. Environmental resistance

Environmental degradation due to moisture, heat and ultraviolet (UV) radiation is of practical concern, particularly to aerospace structures. Carbon fiber epoxy-matrix composites degrade under hygrothermal aging (i.e., aging in the presence of heat and moisture), resulting in a reduction of the mechanical properties. The epoxy absorbs moisture, thus increasing in volume [115] and increasing the contact electrical resistivity of the interlaminar interface of the laminate [116] (Fig. 8).

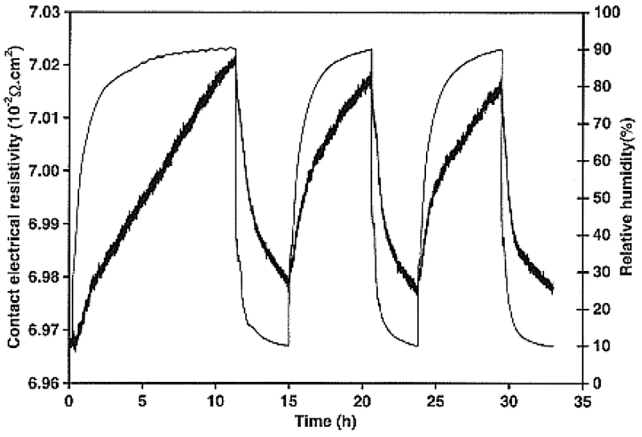

Fig. 8. Variation of the contact electrical resistivity (thick curve) with time and of the relative humidity (thin curve) with time during humidity variation for a continuous carbon fiber epoxy-matrix composite made at a curing pressure of 0.63 MPa. [116].

Compared to epoxy-matrix composites, thermoplastic-matrix composites have less problem with moisture, but they tend to degrade under UV accelerated weathering conditions, with synergistic effects of UV, moisture and heat. Among the thermoplastics, poly(ether-ketone-ketone) (PEKK) is attractive for its high values of the glass transition temperature (T_g), strength, stiffness and fracture toughness, its low moisture absorption, and its good environmental resistance. Nevertheless, UV accelerated weathering condition decreases the storage modulus of a carbon fiber PEKK-matrix composite from 40 to 10 GPa and decreases the T_g from 147 to 105 °C, thereby causing decreases in the modulus and the allowable service temperature [117].

4.13.3. Toughness

Carbon fibers are brittle (low in ductility), though high in tensile strength and modulus. Therefore, a carbon fiber polymer-matrix composite, particularly one with continuous carbon fibers, tends not to be sufficiently tough. (The toughness refers to the energy consumed in fracturing the material.) The polymer matrix is more ductile and tougher than the carbon fiber. However, different polymers differ in their toughness. Therefore, the toughness of a carbon fiber polymer-matrix composite strongly depends on the choice of the polymer matrix. Typically, thermoplastic polymers are tougher than thermoset polymers, because of the highly crosslinked molecular structure of a thermoset and the more linear molecular structure of a thermoplastic polymer. The linear structure allows easy sliding of the molecules relative to one another. The sliding provides a mechanism for consuming the mechanical energy, hence increasing the toughness. Therefore, the use of a thermoplastic polymer instead of a thermoset as the matrix typically enhances both the ductility and the toughness of the composite. Even among the thermosets, the toughness differs [118]. In particular, there are various types of epoxy, which differ in the stiffness (elastic modulus) and toughness. A polymer matrix with high toughness tends to result in a composite with a high impact strength, whereas a polymer matrix with high stiffness tends to result in a composite with a high interlaminar shear strength (ILSS). Thus, a mixture of epoxy resins is commonly used, with the mixture comprising an epoxy that excels in the stiffness and another epoxy that excels in the toughness [119].

4.13.4. Glass transition and melting of the polymer matrix

Thermosets (especially epoxy) have long been used as polymer matrices for carbon fiber composites. During curing, usually performed in the presence of heat and pressure, a thermoset resin hardens gradually, due to the completion of polymerization and the cross-linking of the polymer molecules. Thermoplastic polymers have recently become important because of their greater ductility and processing speed compared to thermosets, and the recent availability of thermoplastic polymers that can withstand relatively high temperatures. The higher processing speed of thermoplastic polymers is due to the fact that thermoplastics soften immediately upon heating above the glass transition temperature (T_g) and the softened material can be shaped easily. Subsequent cooling completes the processing. In contrast, the curing of a thermoset resin is a reaction that occurs gradually.

Thermoplastic polymers soften (with the elastic modulus decreasing) upon heating above their glass transition temperature (T_g) and melt at the melting temperature (T_m), which is an even higher temperature. The glass transition temperature is defined as the temperature at which a thermoplastic polymer softens upon heating. It is also the temperature at which the polymer stiffens upon cooling. This temperature depends on the molecular structure of the polymer. For example, it is −105 °C for low-density polyethylene, −20 °C for atactic polypropylene, 0 °C for isotactic polypropylene (PP), 81 °C for polyvinyl chloride (PVC), and 95 °C for polystyrene (i.e., polyvinyl benzene, PS). The glass-transition temperature can be increased by the presence of carbon fibers, as shown for the case of an acrylonitrile–styrene–acrylate copolymer, the T_g of which is increased from 120.6 to 125 °C by the addition of short carbon fibers [120].

The softening/melting allows fast shaping of composite articles, including the making of foams [121]. The shaping is more versatile for short fiber composites than continuous fiber composites. In contrast, thermosetting resins take time to complete the polymerization. Thus, the turn-around time for manufacturing is shorter for thermoplastic composites than thermosetting composites. Furthermore, the softening/melting enables the joining of thermoplastic components by welding [122]. In contast, thermosetting polymers that have completed polymerization do not soften upon heating and hence are not amenable to welding.

Consider as an example a continuous carbon fiber polymer-matrix composite with the matrix being nylon-6, which is a thermoplastic polymer with glass transition temperature (T_g) 40–60 °C and the melting temperature (T_m) 220 °C. The fiber diameter is 6.9 μm. The fiber weight fraction in the prepreg is 62%. The composite consists of a single prepreg sheet, i.e., a single lamina. The prepreg thickness is 250 μm. Fig. 9 shows the effect of heating through the glass transition temperature and the melting temperature on the behavior of continuous carbon fiber nylon-6-matrix composites that have been annealed prior to this heating at various temperatures for 30 h [123].

Fig. 9(a) shows the heat flow, as recorded by differential scanning calorimetry (DSC). For the 30-h annealing temperature of 150 °C (curve b of Fig. 9(a)), the DSC thermogram shows two endothermic melting peaks with peak temperatures of 171.6 and 216.0 °C. The lower temperature peak may be because of the structural reorganization during annealing, in which the amorphous portion partly developed crystallinity. As the annealing temperature increases to 180 °C (curve c of Fig. 9(a)), the high-temperature peak shifts to a lower temperature and the low-temperature peak shifts to a higher temperature. The height of the low-temperature peak increases while that of high-temperature peak decreases. As the annealing temperature increases to 200 °C (curve d of Fig. 9(a)), the low-temperature peak shifts to a still higher temperature, while its height increases further. The high-temperature peak becomes a shoulder. After annealing at 250 °C (curve e of Fig. 9(a)), no DSC peak was observed. These effects are probably due to the reorganization and thermal oxidative degradation of the nylon-6 matrix, as explained below. Typically the low-temperature melting peak is attributed to the melting of

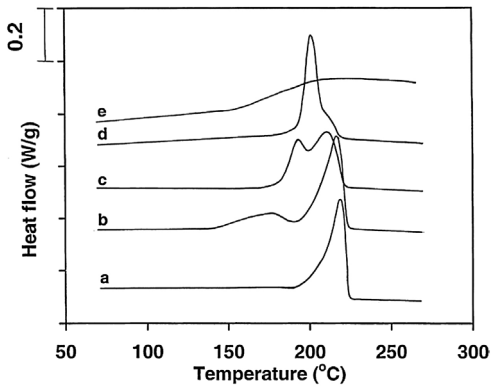

(a)

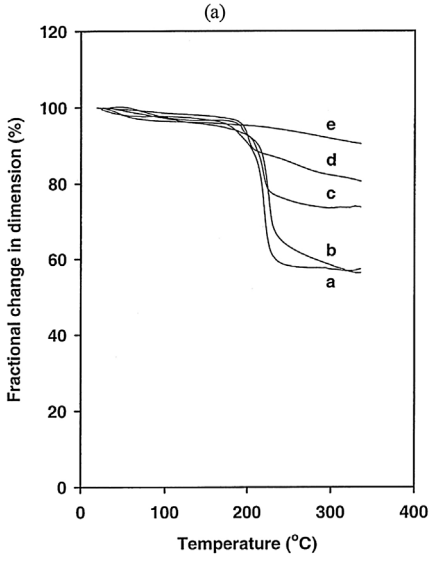

(b)

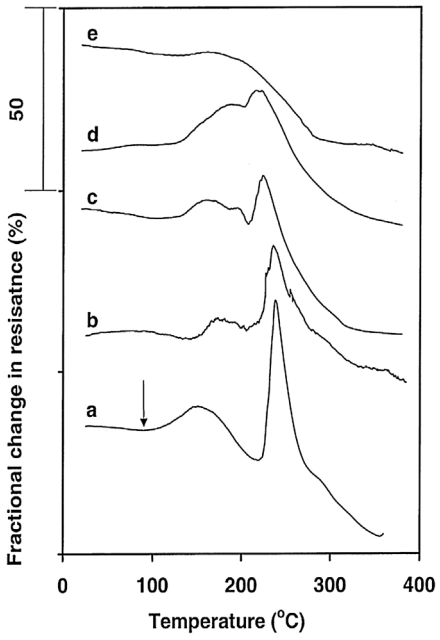

(c)

Fig. 9. The effects of the glass transition and melting on a one-lamina unidirectional continuous carbon fiber thermoplastic polymer-matrix composite. The polymer is nylon-6. The effect of prior annealing for 30 h at various temperatures is shown by the five curves in each graph. Curve a is for the absence of prior annealing. Curve b is for annealing at 150 °C. Curve c is for annealing at 180 °C. Curve d is for annealing at 200 °C. Curve e is for annealing at 250 °C. (a) Plot of the heat flow vs. temperature during heating, with the heat flow measured by differential scanning calorimetry (DSC). (b) Plot of the fractional change in composite thickness vs. temperature during heating, with the thickness measured by using a thermomechanical analyzer (TMA). (c) Plot of the fractional change in the electrical resistance in the fiber direction of the composite vs. temperature during heating. [123].

the portion that has reorganized during annealing. The lower melting temperature increases as the annealing temperature increasea. As the annealing temperature increases from 150 to 200 °C, the portion that has reorganized during annealing increases, thus causing the height of the low-temperature peak to increase. However, as the annealing temperature increases, the extent of degradation increases due to thermal oxidation, which occurs during annealing at a high temperature, thus resulting in lower crystalline perfection. Therefore, the high-temperature peak shifts to a lower temperature and its height decreases. When the annealing temperature is too high (250 °C), the extent of degradation is so great that the melting of the crystalline phase was not observed (curve e of Fig. 9(a)).

Fig. 9(b) shows the effect on the thickness of the composite. For the case of no prior annealing (curve a of Fig. 9(b)), the dimension startes to decrease at 215 °C, due to the softening of the nylon-6 matrix. As the annealing temperature increases, the decrease in dimension is smaller (curves b, c and d of Fig. 9(b)). When the annealing temperature increases to 250 °C, no decrease in dimension was observed (curve e of Fig. 9(b)). This is consistent with the DSC result (curve e of Fig. 9(a)). When the annealing temperature increases, the extent of degradation due to thermal oxidation increases, thus resulting in less decrease in dimension during melting.

Fig. 9(c) shows the effect on the electrical resistance. For the case of no prior annleaing (curve a of Fig. 9(c)), two peaks were observed. The onset temperature of the first peak is 90 °C and that of the second peak is 220 °C. The first peak is attributed to matrix molecular movement above T_g; the second peak is attributed to matrix molecular movement above T_m. When the temperature is above T_g or T_m, the resistance increases due to matrix molecular movement. At the same time, thermal stress, which is due to the thermal expansion mismatch between fiber and matrix, begins to be relieved, resulting in the decrease of the resistance. The latter effect dominates as the temperature increases. The combination of these two effects causes a peak in the resistance versus temperature plot. As a result, two resistance peaks with onset temperatures at T_g and T_m were observed. Because the molecular movement above T_g is less drastic than that above T_m, the first peak is much lower than the second one. Curves b, c and d of Fig. 9(c) show the effect of the annealing temperature. After annealing at 150 °C for 30 h (curve b of Fig. 9(c)), the peak due to molecular movement above T_g disappears. A new peak with an onset temperature of 150 °C appears. This is consistent with the DSC results (cirve b of Fig. 9(a)). This new peak is probably partly attributed to the melting of the crystalline phase that has reorganized during annealing and partly attributed to the melting of the crystalline phase, which has lower perfection than that associated with the main melting peak at the higher temperature. Because the crystalline portion has constraint on the molecular mobility, the molecular movement above T_g is inhibited by the crystalline phase formed during annealing. When the annealing temperature is increased to 180 °C (curve c of Fig. 9(c)), an intermediate-temperature peak with an onset temperature of 180 °C appears, while the height of the high-temperature peak decreases. The melting temperature of the crystalline phase that has reorganized during annealing increases with the annealing temperature. Hence, the portion of the low-temperature peak of curve b of Fig. 9(c) that is due to the melting of the reorganized crystalline phase shifts to a higher temperature and separates from

the portion of the low-temperature peak associated with the melting of the crystalline phase that has lower perfection, thereby resulting in the intermediate-temperature peak with an onset temperature of 180 °C. As the annealing temperature is increased to 200 °C (curve d of Fig. 9(c)), the height of the intermediate-temperature peak increases and this peak overlaps with the peak associated with the melting of the crystalline phase that has lower perfection (i.e., the low-temperature peak). The intermediate-temperature peak also overlaps with the high-temperature peak while the height of the high-temperature peak decreases further. As the annealing temperature is increased to 250 °C (curve e of Fig. 9(c)), no peak was observed. This is consistent with the DSC and TMA results (curve e of Fig. 9(a) and curve e of Fig. 9(b)). However, the resistance decreases as the temperature increases, due to thermal stress relief.

The electrical resistance measurement gives more information on the melting of the polymer matrix than TMA. In particular, the melting of the reorganized crystalline phase and that of the original crystalline phase were more clearly distinguished by resistance measurement than by TMA. The electrical resistance measurement is more sensitive to the glass transition of the polymer matrix than DSC.

The glass transition temperature of a continuous carbon fiber polyamide-matrix composite is increased by the improvement of the fiber-matrix bond through the treatment of the fiber with a coupling agent. The effect of the coupling agent is greater than that of air oxidation of the fiber [23].

4.14. Effects of z-pinning

The combination of (i) pinning in the z-direction (the through-thickness direction) using carbon z-pins (~280 μm diameter, 0.5 vol.%, 3.5 mm spacing, made of a unidirectional carbon fiber bismaleimide-matrix composite) and (ii) the incorporation of CNFs (1 wt.% in the matrix epoxy resin, 70–200 nm diameter, 50–200 μm length) in the epoxy matrix improves the interlaminar fracture toughness of the continuous carbon fiber (woven fabric) epoxy-matrix composite. The CNFs promote the Mode I delamination resistance (~70% increase in the interlaminar fracture energy by toughening around the crack tip). The carbon z-pins, together with the crossover continuous fibers, provide crack bridging behind the crack tip (~200% increase in the fracture energy). In synergy, the two toughening mechanisms result in ~400% increase in the fracture energy. In addition, the delamination fatigue resistance is improved. However, the tensile strength is slightly decreased [124].

4.15. Effect of coatings

The coatings in this section refer to those on the composite rather than those on the fiber. They affect the elevated temperature resistance and in-plane thermal conductivity, as described below.

4.15.1. Elevated temperature resistance

The coating of a unidirectional continuous carbon fiber bismaleimide (BMI) composite laminate with silver (deposited by thermal evaporation), alumina (deposited by electron-beam evaporation) or titanium (deposited by electron-beam evaporation) improves the ability of the composite to withstand elevated temperatures, as tested at 177 °C up to 505 h. Among these coatings, the extent of improvement is greatest for silver, intermediate for alumina and least for titanium. The presence of a chromium interlayer between the coating and the substrate (composite) and the roughening of the substrate surface by sandblasting help the bond of the coating to the substrate [125].

The oxidation resistance of a carbon fiber polymer-matrix composite is improved by using a Y_2O_3-ZrO_2-SiO_2 coating deposited by using an electro-plasma process that involves an electrolyte comprising a mixture of $Y(NO_3)_3$ (the precursor for Y_2O_3) and $Zr(NO_3)_4$ (the precursor for ZrO_2) at 0.1 mol/L, with SiO_2 nanoparticles (80 nm average size) dispersed in the electrolyte at a concentration of 5 g/L, which corresponds to 15 wt.% SiO_2 in the coating. The conversion of $Zr(NO_3)_4$ to ZrO_2 involves the reactions

$$Zr(NO_3)_4 \rightarrow Zr^{4+} + 4NO_3^-$$

$$Zr^{4+} + OH^- \rightarrow Zr(OH)_4$$

$$Zr(OH)_4 \rightarrow ZrO_2 + H_2O \text{ (during plasma discharge)}$$

The reactions are similar for the conversion of $Y(NO_3)_3$ to Y_2O_3. The coating is dense and renders good oxidation resistance to the composite at 1000 °C [126].

4.15.2. In-plane thermal conductivity

The in-plane thermal conductivity of a continuous carbon fiber epoxy-matrix laminate can be increased by the coating of the laminate with a highly-oriented graphite film. The film is made by carbonizing and graphitizing a polymer film. For a film of thickness 70 μm, the density is 1.08 g/cm^3 and the thermal conductivity is 700 W/(m.K) in the in-plane direction and 15 W/(m.K) in the through-thickness direction. The coating of a laminate with the 70-μm thick film by using an adhesive causes the in-plane thermal conductivity of the laminate to increase from 1 to 51 W/(m.K) for a laminate with T700 carbon fiber and from 30 to 119 W/(m.K) for a laminate with M55J carbon fiber [77].

4.16. Effect of strain on the electrical resistivity

The electromechanical behavior of carbon fiber polymer-matrix composites mainly pertains to the effect of mechanical strain or stress on the electrical resistivity. This effect is known as piezoresistivity, which stems from the effect of the strain or stress on the microstructure, which in turn affects the electrical resistivity. The type of microstructural change depends on the structure of the composite. Piezoresistivity allows electrical-resistance-based sensing of strain, which relates to the stress in the elastic regime through the elastic modulus.

The electrical resistance R is related to the resistivity ρ by the basic equation

$$R = \rho l/A, \tag{14}$$

where l is the length of the specimen in the direction of resistance measurement A is the cross-sectional area in the plane perpendicular to the direction of resistance measurement. Taking the natural logarithm of Eq. (14) and then the derivative gives

$$(\Delta R)/R = (\Delta \rho)/\rho + (\Delta l)/l - (\Delta A)/A. \tag{15}$$

The two dimensions w_1 and w_2 that define the area $A = w_1 w_2$ are given by

$$(\Delta w_1)/w_1 = -\nu_{12} (\Delta l)/l, \tag{16}$$

and

$$(\Delta w_2)/w_2 = -\nu_{13} (\Delta l)/l, \tag{17}$$

where ν_{12} and ν_{13} are the values of the Poisson's ratio in the w_1 and w_2 directions, respectively. In case that the material is isotropic, ν_{12} and ν_{13} are equal and let the value be ν. Hence, for an isotropic material, Eq. (17) becomes

$$(\Delta R)/R = (\Delta\rho)/\rho + [(\Delta l)/l]\ (1 + 2\boldsymbol{\nu}). \quad (18)$$

For a material that is not piezoresistive, $(\Delta\rho)/\rho = 0$ in Eq. (18). For a piezoresistive material, $(\Delta R)/R$ is approximately equal to $(\Delta\rho)/\rho$ if $(\Delta l)/l$ is very small, as in the case of a material with a high value of the elastic modulus.

The gage factor (F) is defined as the fractional change in resistance per unit strain. Hence,

$$F = [(\Delta R)/R]/[(\Delta l)/l]. \quad (19)$$

For an isotropic material that is not piezoresistive, the combination of Eq. (18) and (19) gives

$$F = 1 + 2\nu. \quad (20)$$

In case that $(\Delta\rho)/\rho$ in Eq, (18) is negative, it is possible for the gage factor F to be negative.

Positive piezoresistivity refers to the behavior in which the resistivity increases with increasing strain, i.e., $(\delta\rho/\rho)/(\delta\ell/\ell) > 0$; negative piezoresistivity refers to the behavior in which the resistivity decreases with increasing strain, i.e., $(\delta\rho/\rho)/(\delta\ell/\ell) < 0$. Piezoresistivity is usually positive. It should be noted that the strain is positive for elongation and negative for shrinkage. A material that exhibits positive piezoresistivity has its resistivity increase upon tension and decrease upon compression.

For a strain sensor that is not piezoresitive, but provides strain sensing due to the effect of the dimensional changes alone on the resistance, the gage factor is about 2, with the exact value depending on the Poisson's ratio. However, for a piezoresistive strain sensor, the gage factor is greater than 2. For example, the gage factor is as high as 37 for a carbon fiber epoxy-matrix composite [127].

For a composite laminate with continuous carbon fibers, the piezoresistivity can be positive or negative, stemming from the effect of strain on the extent of contact among the fibers. For example, the flexure of a laminate beam causes the surface resistance of the tension surface of the beam to increase (due to the decreasing contact among the fibers and the consequent decrease in the degree of current penetration from the surface) and causes the surface resistance of the compression surface of the beam to decrease (due to the increasing contact among the fibers and the consequent increase in the degree of current penetration from the surface) (Fig. 10) [128,129].

The surface resistance does not simply relate to the volume resistance, because the depth of current penetration from the surface is unclear. However, the surface resistance can be calculated by using an equivalent circuit model [130].

The flexural effects shown in Fig. 10 have been confirmed under a pure bending moment [131]. In addition, the effect of the flexure on the resistance of the tension surface has been confirmed for a continuous carbon fiber epoxy-matrix composite that is bonded to a glass fiber epoxy-matrix composite substrate [132]. Furthermore, the effects of flexure on both tension and compression surfaces have been confirmed for a carbon fiber mat epoxy-matrix laminate bonded to both sides of a continuous glass fiber composite beam under flexure [133]. In addition, for this mat laminate bonded to a continuous fiber composite, it has been reported that the resistance in the force direction increases upon pure in-plane shear, with a gage factor (fractional change in resistance per unit shear strain) of only 1.7 [133].

For a unidirectional continuous carbon fiber epoxy-matrix composite under uniaxial longitudinal tension, the longitudinal resistance increases reversibly (with gage factor = −36, indicating negative piezoresistivity), while the through-thickness resistance decreases reversibly (with gage factor = +34, indicating positive piezoresistivity) (Fig. 11) [127]. The reverse occurs upon uniaxial longitudinal compression. For a crossply composite (rather than a unidirectional composite), the gage factor for the longitudinal resistance is −6 (rather than −36). These effects are attributed to tension straightening the fibers and decreasing the degree of through-thickness fiber–fiber contact, thereby causing the longitudinal resistance to decrease and the through-thickness resistance to increase. The effect of tension on the degree of through-thickness fiber–fiber contact is less for a crossply composite than a unidirectional composite, thus reducing the magnitude of the gage factor.

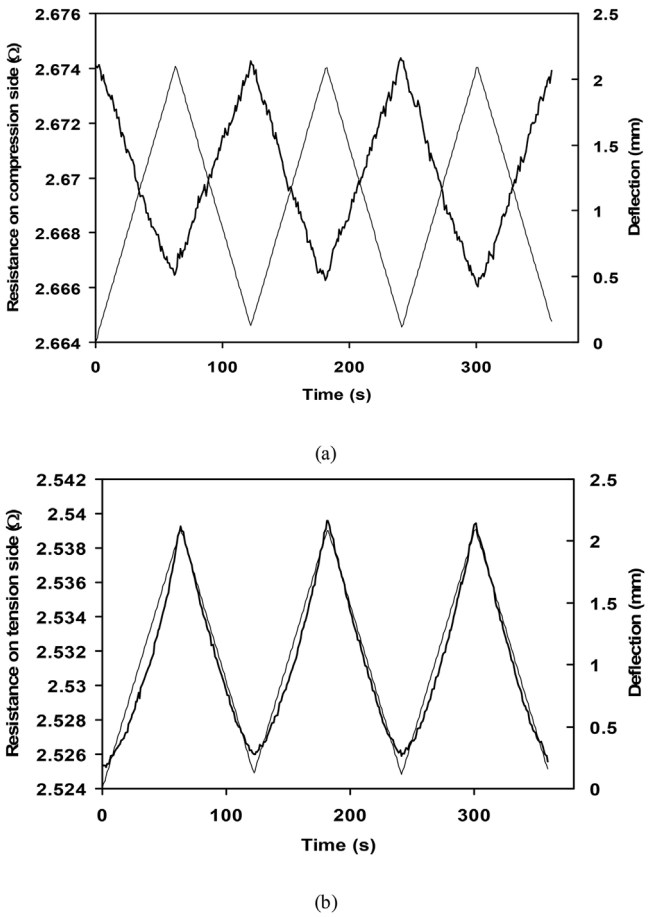

Fig. 10. Surface resistance (thick curve) during deflection (thin curve) cycling at a maximum deflection of 2.098 mm (stress amplitude of 392.3 MPa) for a 24-lamina quasi-isotropic continuous carbon fiber epoxy-matrix composite. (a) Compression surface. (b) Tension surface. [128].

For both the longitudinal resistance and the through-thickness resistance, the slight resistance decrease at the end of the first loading cycle (Fig. 11) is attributed to the disturbance to the fiber arrangement during the first cycle causing an irreversible increase in the degree of fiber–fiber contact. The degree of fiber–fiber contact affects the through-thickness resistance more than the longitudinal resistance.

The gage factor (the reversible fractional change in resistance per unit strain) decreases slightly with increasing strain amplitude. This is due to the increasing extent of the irreversible resistance change [4].

The DC electrical resistance measurement is effective for monitoring the effects of temperature and stress on the interface between a concrete substrate and its continuous carbon fiber epoxy-matrix composite retrofit. The apparent resistance of the retrofit in the fiber direction is increased by bond degradation, whether the degradation is due to heat or stress. The degradation is reversible, in case that it is minor. Irreversible disturbance in the

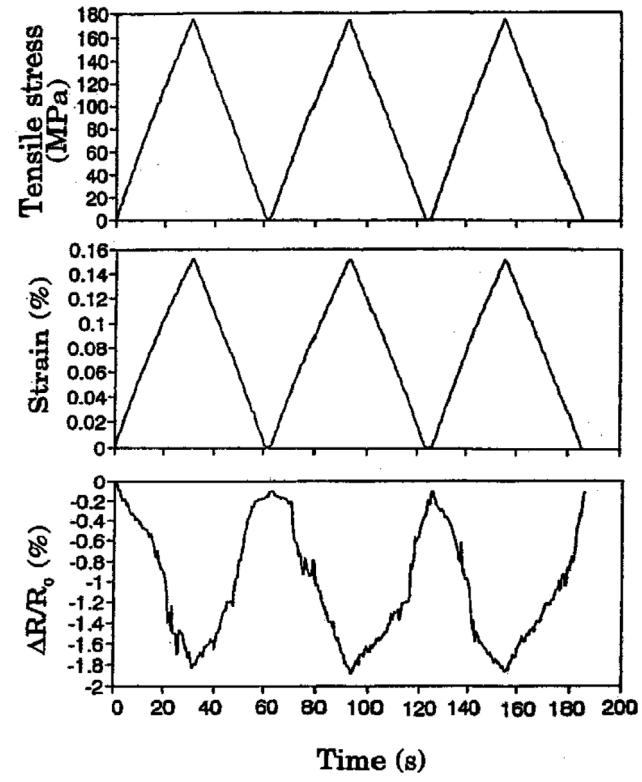

(a)

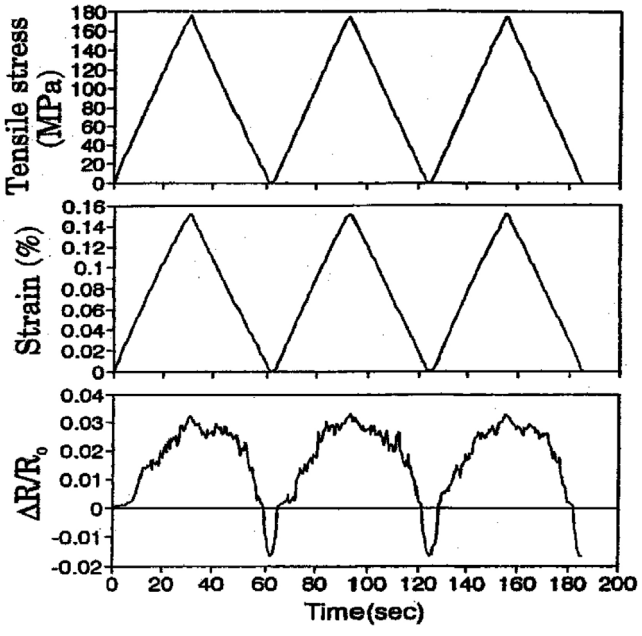

(b)

Fig. 11. Fractional change in the volume resistance during cyclic longitudinal tension of a unidirectional continuous carbon fiber epoxy-matrix composite. (a) Resistance in the longitudinal direction. (b) Resistance in the through-thickness direction. [127].

fiber arrangement occurs slightly as thermal or load cycling occurs, as indicated by the resistance decreasing cycle by cycle [134].

For a single carbon fiber embedded in epoxy, as tested with the two-probe method, such that the two electrical contacts are on the fiber rather than on the epoxy surrounding the fiber, the gage factor under tension is +0.50 and +0.42 for sized and unsized carbon fibers, respectively. In the absence of the epoxy, the similarly tested single fiber gives gage factor +1.58 and +1.31 for sized and unsized fibers, respectively [135]. All these values of the gage factor are small, indicating that the piezoresistivity is very weak. In contrast, for a conventional carbon fiber epoxy-matrix composite with a large number of fibers, the magnitude of the gage factor is much higher, due to the effect of the fiber arrangement on the resistivity of the composite.

4.17. Effect of damage on the electrical resistivity

Damage tends to cause the electrical resistivity of an electrically conductive material to increase, though this is not always the case. For example, the breaking of the conductive fibrous filler (whether discontinuous or continuous) in a composite tends to reduce the electrical connectivity of the filler, thereby increasing the resistivity of the composite. In case of a continuous carbon fiber composite, the resistivity in the longitudinal direction (fiber direction) is particularly sensitive to the fiber breakage. Another type of damage involves matrix cracking, which also tends to reduce the electrical connectivity of the filler, thereby increasing the resistivity of the composite. In case of a continuous carbon fiber composite, the resistivity in the through-thickness direction is particularly sensitive to delamination.

Under uniaxial tension in the longitudinal (fiber) direction, the volume resistance of a carbon fiber composite in this direction irreversibly increases upon damage (Fig. 12(a) and (b)). This is due to fiber breakage [136,137]. The resistance may be measured with the four-probe method, such that each of the four electrical contacts is around the entire perimeter of the specimen in the plane perpendicular to the direction of resistance measurement [136]. Alternatively, the surface resistance (rather than the volume resistance) is measured with four contacts that are all on the same surface.

Damage during mechanical fatigue (specifically tension–tension fatigue with the tension being uniaxial tension in the longitudinal direction) is observed as early as 50% of the fatigue life (Fig. 12(a) and (b)) [136]. The notion that the increase in resistance is associated with damage is supported by the observed decrease in the secant modulus (the instantaneous stress divided by strain at the same time) [136]. The secant modulus decrease accompanies the resistance increase (Fig. 12(b)). This notion is further confirmed by the observation of pulses of acoustic emission during loading [138–140].

Impact damage is practically important, as the impact may be due to a bird or hail striking an aircraft wing, for example. Impact damage tends to be localized, whereas flexural damage and tensile damage tend to be more spread out. The sensing of impact damage in carbon fiber composite can be achieved by surface resistance measurement, which should be directed at a region that contains the point of impact, unless the current spreading from the point of impact is sufficiently large.

For a carbon fiber composite, the resistance (measured by using the four-probe method) increases irreversibly upon impact damage, such that the resistance increases with increasing impact energy above 0.7 J [141–144]. By using the two-probe method, irreversible resistance increase was observed at impact energy above 7 J [145]. This behavior is shown in Fig. 13(a), where the impact energy ranges from 0.73 to 5.08 J and the measured resistance is the oblique resistance [143]. The behavior is similar for oblique, through-thickness and surface resistance, with the surface resistance being either the resistance of the surface receiving the impact or that of the opposite surface. The through-thickness and oblique resistances are more sensitive to the impact damage than the surface resistance (Fig. 13(b)).

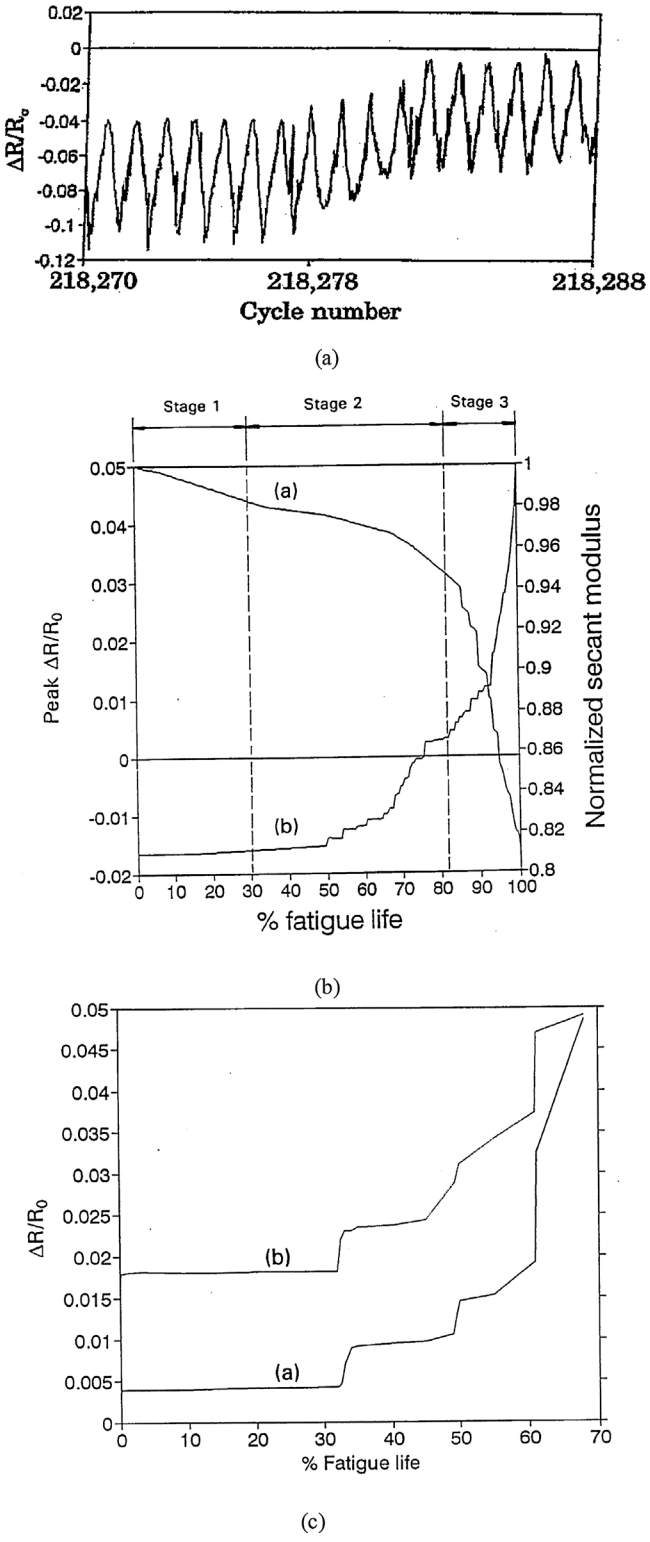

Fig. 12. Evolution of damage during tension–tension fatigue. (a) The longitudinal resistance decreases reversibly in each tensile loading cycle, due to strain (as shown in Fig. 13), but the baseline resistance increases abruptly at a certain point in the fatigue life. This is the first abrupt increase of the resistance and corresponds to the first occurrence of fiber breakage during fatigue. (b) The variation of the longitudinal resistance (the peak resistance of a cycle) during the entire fatigue life. Damage in the form of fiber breakage is shown by this resistance increasing. Curve a: normalized secant modulus. Curve b: the peak value of the fractional change in resistance (relative to the initial resistance) in a stress cycle. (c) The variation of the through-thickness resistance during the entire fatigue life. Damage in the form of delamination is shown by this resistance increasing. Curve a: the minimum value of the fractional change in resistance (relative to the initial resistance) in a stress cycle. Curve b: the maximum value of the fractional change in resistance in a stress cycle. [136].

4.18. Effects of compression on the fastening-relevant interface between contacting unbonded composites

Composite members that are not bonded to one another but are in tight physical contact due to the compressive stress present in the direction perpendicular to the plane of the contact represent a situation that is relevant to the joining of these members by fastening. The interface between two contacting unbonded carbon fiber polymer-matrix composite surfaces can be characterized in terms of the contact electrical resistivity, which is sensitive to the degree and nature of the contact across the interface. As surfaces are never perfectly smooth microscopically, the two surfaces touch each other at points, with each point associated with a contact resistance. Compressive deformation of a hillock corresponding to a contact point increases the area of the point, thereby decreasing the resistance of this point. The local stress at a hillock is much larger than the overall applied stress. Fig. 14 shows that the contact resistance of the overall contact interface decreases upon compression in every compression cycle, such that the resistance decrease is partly reversible and partly irreversible upon unloading. The reversible decrease is due to the elastic deformation of the hillocks, whereas the irreversible decrease is due to the plastic deformation of the hillocks. The plastic deformation is significant in the first three cycles, after which the resistance change becomes essentially totally reversible in each cycle. That the resistance levels off as cycling progresses is because there is a limit to the degree of flattening of the hillocks. Compression in the direction perpendicular to the interface occurs in the joining of composite panels by fastening. Thus, Fig. 14 shows that the fastening and unfastening affect both reversibly and irreversibly the microstructure of the joint [146].

5. Applications

Multifunctionality, smart structures, hierarchical (multi-scale) composites and application broadening are expected to fuel the growth of research in continuous carbon fiber polymer-matrix composites. The applications are addressed in this section.

5.1. Lightweight structure applications

Carbon fiber polymer-matrix composites are mainly used for lightweight structures, due to their combination of low density, high modulus and high strength. Applications include primary and secondary structures of civil and military aircraft [147], satellite components, thin-walled tubing for aircraft and satellites, launch vehicle components, rocket fuel tanks, honeycomb structures [148], armor against ballistic penetration [149], surface-reinforced wood [150], automobile structural components [151–153], missiles, solid-propellant rocket motors, pressure vessels, the backing frame of solar panel systems [154], sporting goods [155] (such as fishing rods, tennis racquets [156] and badminton racquets), race bicycles, cars, and prosthetics. Automotive applications involve thermoplastic-matrix composites for secondary automotive components, and thermoset-matrix composites for car body applications, with future applications of the thermoplastic-matrix composites including crash elements, racing car seats, and the production and recycling of automotive fenders [151]. Carbon fiber composite racquets are stronger and lighter than the wooden ones and, in addition, they can take tighter strings than the wooden ones. The Boeing 787 Dreamliner aircraft utilizes continuous fiber polymer-matrix composites in 50% of the aircraft, with composites constituting 100% of the skin, entire sections of the fuselage, in

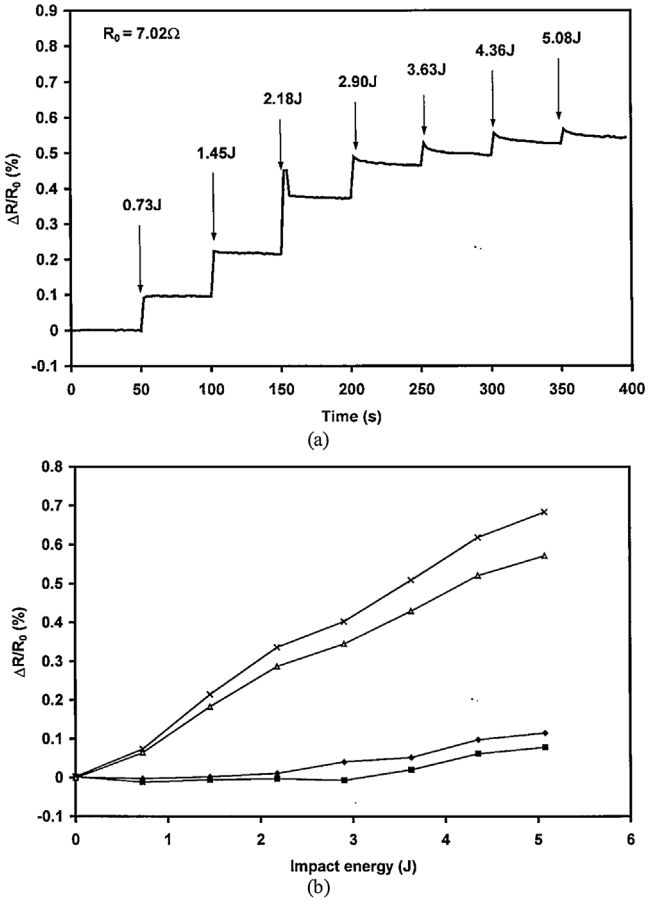

Fig. 13. Effect of impact energy on the electrical resistance. (a) Fractional change in oblique resistance (relative to the initial resistance) versus time during impact at progressively increasing energy for a continuous carbon fiber epoxy-matrix composite. The arrows indicate the times of the impacts. (b) Fractional change in resistance (relative to the initial resistance) vs. time during impact at progressively increasing energy. X: Through-thickness resistance; ▲: Oblique resistance; ◆: Top surface resistance; ■: Bottom surface resistance. The various resistances are simultaneously measured. [143].

addition to the tail, wing box and wing skins. Other aerospace applications include antennas that can bear structural loads [157], satellite platform structural panels and radiators, with demands including low mass, high stiffness, high strength, high operating temperatures, high thermal conductivity, vacuum compatibility, high in-orbit stability, and compatibility with metallic parts [158]. A carbon fiber polymethymethacrylate (PMMA) matrix composite can provide the cementing connection of an endoprosthesis with a bone [159].

5.2. Construction applications

Applications in the construction industry have emerged. In one application, carbon fiber polymer-matrix composites are used as cables. For example, the composite cables are used to anchor an earthquake-resistant building [160]. In another example, carbon fiber polymer-matrix composite cables have been in use since 1996 on the vehicular cable-stayed Stork Bridge with 124-m span in Winterthur, Switzerland [161]. Advantages of these cables include corrosion resistance, high specific strength and stiffness, and excellent fatigue resistance.

Another construction application relates to the use of a continuous carbon fiber polymer-matrix composite as a grid for reinforcing concrete. For example, by using carbon fiber epoxy-matrix composite grids as reinforcement in precast concrete, it is possible to produce concrete facade panels that are only 26 mm thick. The grid consists of two plies of carbon fiber scrim spaced 12 mm apart and connected by compression-resistant pile threads. The carbon fiber is attractive for its corrosion resistance. In contrast, a steel-reinforced concrete facade panel of similar size has a minimum thickness of 100 mm, as necessitated by the prevention of corrosion of the steel due to water ingress through the cracks in the concrete. [162].

In a related application, carbon fiber grid is used to replace welded steel wire mesh in precast concrete for the purpose of reducing weight and enhancing corrosion resistance. Other applications of the grid include concrete countertops, architectural detailing, fireplace surrounds and mantels, sinks, bathtubs and backsplash walls. Carbon fiber grid costs about twice as much as the conventional steel reinforcement that it replaces. However, it enables changes in precast design so that the component cost is similar to that of conventional precast. In particular, the carbon fiber grid requires only 0.25 in (6.35 mm) of concrete cover, compared to steel reinforcement, which typically requires a concrete cover of thickness ranging from 0.25 in (19 mm) to 1.5 in (38 mm) to provide sufficient protection from moisture-induced corrosion. Moreover, the carbon fiber grid controls shrinkage cracks up to 50% more effectively than steel mesh [163]. On the other hand, carbon fiber competes with glass fiber, which is less expensive, though glass fiber is inferior to carbon fiber in the elastic modulus and chemical durability.

Yet another construction application relates to the use of the continuous carbon fiber polymer-matrix composite for the repair or retrofitting of concrete or masonry. In one example, the composite in the form of a sheet (which is flexible, since the resin has not yet cured) is wrapped around the concrete column or is applied on a concrete surface, followed by curing. Such repair or retrofitting is needed for a large variety of applications, such as bridge and overpass reinforcement (for the purpose of increasing the load tolerance), the support of building steeples (because of under-designed wind loads), parking garages (to restore structural integrity), brick buildings (to increase the shear capacity), highway repair (to waterproof segmental joints), home foundations (to repair fractured foundations), and new construction (to increase the wind load tolerances not considered during construction) [164]. In another example, the composite in the form of a cylindrical shell (rigid because the resin has been cured) of diameter larger than the concrete column is placed in two halves around the column and then concrete is poured between the shell and the column [165].

5.3. Non-structural applications

Carbon fiber polymer-matrix composites are used for computer casings due to their high effectiveness for EMI shielding [166].

Flexible devices for wearable electronics are enabled by using carbon fiber yarns [167] or carbon fiber paper [168]. A hybrid yarn involving a carbon fiber yarn at the core and an electrically insulting yarn material (e.g., polymer, glass, etc.) coating the core yarn is attractive for functional composite applications that require the electrical insulation [169].

Carbon fibers can be coated with a porous layer of MnO_2 for use as supercapacitor electrodes [170]. Similarly, carbon fibers can have a pseudo-capacitive material in the form of aligned metal oxide nanowires grown on them for the purpose of increasing the electrode-electrolyte contact area and the ion diffusion rate [171].

Other emerging applications of carbon fiber polymer-matrix composites are becoming increasingly important. They include (i) alternative energy, such as wind turbines [172,173] (with lighter turbine blades enabled by the use of carbon fiber resulting in gear

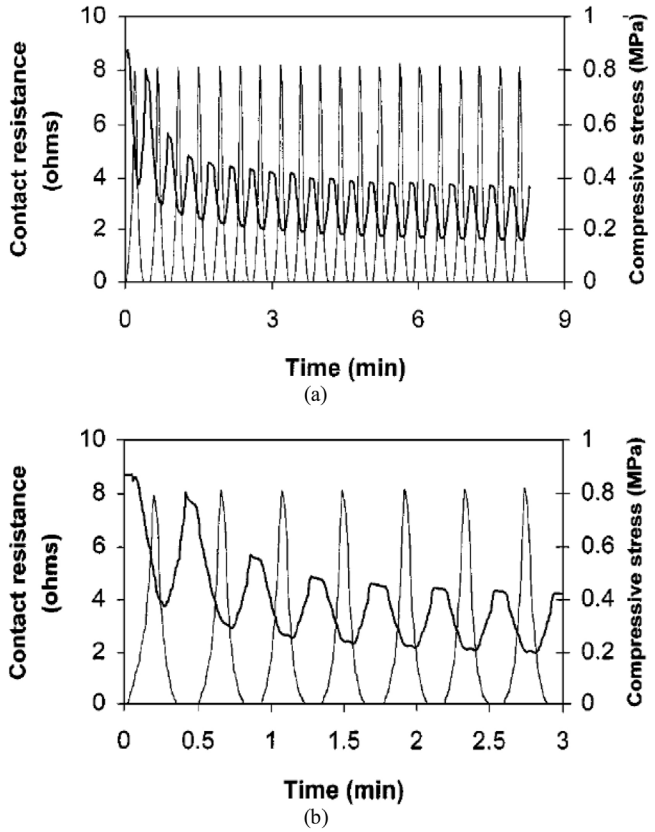

Fig. 14. The contact electrical resistivity (thick curve) of the interface between two pieces of continuous carbon fiber polymer-matrix composite that are subjected to a cyclic compressive stress (thin curve) applied in the direction perpendicular to the interface. The polymer is Nylon-6, a thermoplastic polymer. The fibers are unidirectional. (a) The overall cyclic testing. (b) The first 7 cycles. [146].

box, tower and foundation that are lighter), flywheel energy storage, compressed natural gas storage and transportation, and high-pressure hydrogen tanks for fuel cell-powered automobiles [174], (ii) fuel efficient automobiles, (iii) construction and infrastructure, such as lightweight pre-cast concrete, concrete reinforcement [175], concrete repair [176,177], the anodic material for the cathodic protection of steel reinforced concrete [178], earthquake protection, steel reinforcement [179,180] and aluminum reinforcement [181], (iv) oil exploration, such as deep sea drilling platforms, buoyancy, umbilical, choke, kill lines and drill pipes [182], (v) solar panel support [154], and (vi) biomaterials [183].

The use of lightweight materials such as composite materials in wind turbine blades helps reduce the rotational inertia, so that the turbines can accelerate quickly when the wind picks up, For cost saving, glass fibers rather than carbon fibers are typically used for wind turbines. However, for large turbines, carbon fibers are increasingly being used [172]. In addition, carbon fiber composites are attractive for their electrical conductivity, which enables the deicing of the wind turbines by resistance heating [184].

Compared to the widely used carbon fiber thermoset-matrix composites (commonly with epoxy as the thermoset), carbon fiber thermoplastic-matrix composites are advantageous in their reworkability, which is a consequence of the ability of the thermoplastic matrix to melt upon heating. In addition, the thermoplastic composites are attractive for their greater toughness, which is a consequence of the relative ease of sliding between the adjacent molecules in a thermoplastic polymer. In addition to conventional structural applications, carbon fiber thermoplastic composites with continuous fibers are used in the form of pellets for reinforcing thermoplastic polymer articles.

The decrease in the price of carbon fibers will widen the applications of this material. In particular, the high cost of carbon fibers compared to other materials deters the use of carbon fiber composites in transportation. Therefore, there is much interest in lowering the cost of manufacturing carbon fibers [185]. The carbon fiber precursor costs much more than the other costs. Therefore, attention should be directed at the precursor for the purpose of reducing the manufacturing cost. An example of a low-cost precursor is lignin, which is a wood-based product [186]. Another example is a textile-grade acrylic fiber, the conversion of which to carbon fiber has been developed by the U.S. Oak Ridge National Laboratory [187].

The global carbon fiber market size, in terms of value, is projected to reach US$3.51 billion by 2020, at a compounded annual growth rate (CAGR) of 9.1% between 2015 and 2020. The global carbon fiber reinforced plastic (CFRP) market is projected to reach USD 35.75 Billion by 2020, at a CAGR of 9.9% between 2015 and 2020 [188].

6. Conclusion

The processing-structure-property relationships of continuous carbon fiber polymer-matrix composites have been reviewed, due to the importance of these relationships to the design, tailoring and development of these materials. Numerous processing/structure parameters are considered in terms of their effects on the properties, which include structural, thermal and functional properties. In addition, this paper reviews the rapidly broadening applications, which have extended beyond aircraft structures and help fuel the growth of the field.

The curing pressure and fiber lay-up configuration affect the static and dynamic mechanical properties, fatigue resistance and through-thickness thermal conductivity. The fiber type affects the CTE, thermal conductivity, dielectric properties, EMI shielding effectiveness and thermoelectric power. The filler addition affects the ablation and fire resistance, static and dynamic mechanical properties, toughness, electrical conductivity, CTE, in-plane and through-thickness thermal conductivity, and through-thickness thermoelectric behavior. The interlayers between laminae affect the toughness, viscous behavior, electrical conductivity, wear resistance, self-healing ability, fire resistance, thermal conductivity, CTE, and dielectric properties. The polymer matrix affects the elevated temperature and environmental resistance, toughness, matrix glass transition, and matrix melting. The composite coatings affect the elevated temperature resistance and in-plane thermal conductivity. The temperature affects the fatigue resistance and viscoelastic behavior. The strain and damage affect the electrical conductivity. Through-thickness compression affects the fastening-relevant interface between contacting unbonded composites.

Funding

This research did not receive any specific grant from funding agencies in the public, commercial, or not-for-profit sectors.

References

[1] B.T. Kelly, P.L. Walker Jr., Carbon 8 (1970) 211–226.
[2] M. Kuribara, H. Nagano, J. Electr. Cool. Thermal Control 5 (2015) 15–25.
[3] K. Morioka, Y. Tomita, Mater. Charact. 45 (2000) 125–136.
[4] D. Wang, D.D.L. Chung, Carbon 60 (1) (2013) 129–138.
[5] R. Richardson, Int. SAMPE Tech. Conf. (2010) (a53/1-a53/10).
[6] C. McHugh, SAMPE J. 45 (6) (2009) 33–43.

[7] C. McHugh, SAMPE Conf. Proc. 55 (SAMPE 2010) (2010) (mchug1/1-mchug1/16).
[8] M. Ramirez, D.D.L. Chung, Carbon (2016) (in press).
[9] J. Wu, D.D.L. Chung, Carbon 42 (14) (2004) 3039–3042.
[10] S. Han, D.D.L. Chung, J. Mater. Sci. 47L (2012) 2434–2453.
[11] Y. Hirano, T. Yamane, A. Todoroki, Compos. Sci. Technol. 122 (2016) 67–72.
[12] F. Ahmed, B.S. Lalia, V. Kochkodan, N. Hilal, R. Hashaikeh, Desalination 391 (2016) 1–15.
[13] S. Han, D.D.L. Chung, Appl. Clay Sci. 83–84 (2013) 375–382.
[14] S. Putić, P.S. Uskoković, R. Aleksić, Strength Mater. 35 (5) (2003) 500–507.
[15] P.N.B. Reis, J.A.M. Ferreira, J.D.M. Costa, M.O.W. Richardson, Compos. Sci. Technol. 69 (2009) 154–160.
[16] W.K. Goertzen, M.R. Kessler, Compos. Part B 38B (1) (2006) 1–9.
[17] S. Han, D.D.L. Chung, Compos. Sci. Technol. 71 (16) (2011) 1944–1952.
[18] S. Han, D.D.L. Chung, Compos. Part A 48 (2013) 162–170.
[19] S. Han, D.D.L. Chung, Carbon 52 (2013) 30–39.
[20] D.H. Sung, G. Kang, K. Kong, M. Kim, H.W. Park, Y. Park, Compos. Part B 92 (2016) 202–209.
[21] M. Kuribara, H. Nagano, J. Electron. Cool. Thermal Control 5 (2015) 15–25.
[22] L.E. Evseeva, S.A. Tanaeva, Mech. Compos. Mater. 49 (2) (2013) 155–162.
[23] W.Z. Nie, J. Li, Y.C. Xia, Plastics Rubber Compos. 9 (1) (2010) 21–24.
[24] C. Zweben, SAMPE Conf. Proc. 54 (2009) (zwebe1/1-zwebe1/10).
[25] X. Liu, R. Wang, Z. Wu, W. Liu, J. Compos. Mater. 48 (9) (2014) 1143–1151.
[26] D.D.L. Chung, Carbon 50 (2012) 3342–3353.
[27] D.D.L. Chung, J. Mater. Sci. 39 (8) (2004) 2645–2661.
[28] M. Rahaman, T.K. Chaki, D. Khastgir, Polym. Compos. 32 (11) (2011) 1790–1805.
[29] J. Wu, D.D.L. Chung, Carbon 40 (ER3) (2002) 445–447.
[30] J.W. Fergus, J. Eur. Ceramic Soc. 32 (3) (2012) 525–540.
[31] A.D. LaLonde, Y. Pei, H. Wang, G.J. Snyder, Mater. Today (Oxford, United Kingdom 14 (11) (2011) 526–532.
[32] M. Ohtaki, J. Ceramic Soc. Jap. 119 (2011) 770–775.
[33] S. Wang, D.D.L. Chung, Compos. Interfaces 6 (6) (1999) 519–530.
[34] H. He, F. Gao, Int. J. Polym. Anal. Character. 20 (2) (2015) 180–189.
[35] D.Q. Dao, T. Rogaume, J. Luche, F. Richard, L. Bustamante Valencia, S. Ruban, Fire Mater. 40 (1) (2016) 27–47.
[36] T.A. Lenda, S. Mridha, Adv. Mater. Res. 264–265 (2011) 451–456.
[37] A.Y. Malkin, A.I. Isayev, Rheology—Concepts, Methods, & Applications, ChemTec Publishing, Toronto, 2006.
[38] J. Tomioka, K. Kiguchi, Y. Tamura, H. Mitsuishi, Int. J. Hydrogen Energy 36 (3) (2011) 2513–2519.
[39] D.D.L. Chung, J. Mater. Sci. 36 (2001) 5733–5738.
[40] W. Fu, D.D.L. Chung, Polym. Polym. Compo. 9 (6) (2001) 423–426.
[41] H. Dhieb, J.G. Buijnsters, K. Elleuch, J.P. Celis, Compo. Part B 88 (2016) 240–252.
[42] R.L. Clark III, M. Skinner, B. Farah, J. Farris, K.T. Hsiao, M.R. Parker, Pp, Proc. 53rd Int. SAMPE Symp. Exhib. Society for the Advancement of Material and Process Engineering, Covina, CA, 2008, pp. 152/1–152/11.
[43] L. Gao, E.T. Thostenson, Z. Zhang, T. Chou, Adv. Funct. Mater. 19 (1) (2009) 123–130.
[44] S. Wang, J. Qiu, Compos. Part B 41 (2010) 533–536.
[45] J. Zhu, A. Imam, R. Crane, K. Lozano, V.N. Khabashesku, E.V. Barrera, Compos. Sci. Technol. 67 (2007) 1509–1517.
[46] D. Yang, W. Zhang, B. Jiang, Ceramics Int. 39 (2) (2013) 1575–1581.
[47] M. Rallini, M. Monti, M. Natali, J.M. Kenny, L. Torre, Int SAMPE Technical Conf. 43(Developing Scalable Materials and Processes for Our Future) (2011) Rallini1/1–Rallini1/9.
[48] M. Rallini, M. Natali, M. Monti, J.M. Kenny, L. Torre, Fire Mater. 38 (3) (2014) 339–355.
[49] A. Faingold, M. Narkis, A. Siegmann, J. Macromol. Sci. Part B 47 (3) (2008) 485–499.
[50] B.Z. Jang, J.Y. Liau, L.R. Hwang, W.K. Shih, J. Reinf, Plastics Compos. 9 (1990) 314–321.
[51] A.G. Mamalis, N. Pantelelis, K. Spentzas, N. Efentakis, Congresso Anual da ABM, Volume 65th(2010) , pp. 4568–4576.
[52] N. Athanasopoulos, G. Koutsoukis, D. Vlachos, V. Kostopoulos, Compos. Part B 50 (2013) 279–289.
[53] N. Athanasopoulos, V. Kostopoulos, Compos. Part B 42B (6) (2011) 1578–1587.
[54] H. Zhao, L. Wang, X. Zhao, J. Su, J. Comput. Theor. Nanosci. 5 (8) (2008) 1685–1687.
[55] Q. Chen, Y. Zhao, Z. Zhou, A. Rahman, X. Wu, W. Wu, T. Xu, H. Fong, Compos. Part B 44 (1) (2013) 1–7.
[56] J.A. VanderVennet, T. Duenas, Y. Dzenis, C.T. Peterson, C.E. Bakis, D. Carter, J.K. Roberts, Proceedings of SPIE 7978(Behavior and Mechanics of Multifunctional Materials and Composites 2011) (2011) 797823/1–797823/10.
[57] C.H. Zhang, Z.Q. Zhang, H.L. Cao, Diffusion and Defect Data–Solid State Data, Pt. B, 121–123(Pt. 2, Nanoscience and Technology, Part 2) (2007) 1253–1256.
[58] Y. Mebarki, S. Rechak, D. Marc, A. Maslouhi, J. Braz. Soc. Mech. Sci. Eng. 36 (4) (2014) 939–949.
[59] S. Kobayashi, J. Kitagawa, Compos. Part B 85 (2016) 31–40.
[60] S. Fang, D.D.L. Chung, Composites 21 (5) (1990) 419–424.
[61] X.R. Wang, X.Q. Wu, M.L. Liu, Polym. Polym. Compos. 20 (1 & 2) (2012) 161–163.
[62] S. Sprenger, M.H. Kothmann, V. Altstaedt, Compos. Sci. Technol. 105 (2014) 86–95.
[63] S.W. Hudnut, D.D.L. Chung, Carbon 33 (11) (1995) 1627–1631.
[64] M. Chua, C. Chui, IEEE Trans. Nanotechnol. 14 (2) (2015) 363–371.
[65] R.M. Lin, C. Lu, Mech. Syst. Signal Proc. 24 (2010) 2996–3012.
[66] J. Simitzis, L. Zoumpoulakis, S. Soulis, D. Triantou, C. Pinaka, J. Appl. Polym. Sci. 121 (4) (2011) 1890–1900.
[67] D.K. Chakravarthi, V.N. Khabashesku, R. Vaidyanathan, J. Blaine, S. Yarlagadda, D. Roseman, Q. Zeng, E.V. Barrera, Adv. Funct. Mater. 21 (13) (2011) 2527–2533.
[68] A. Shah, Y. Wang, H. Huang, L. Zhang, D. Wang, L. Zhou, Y. Duan, X. Dong, Z. Zhang, Compos. Struct. 131 (2015) 1132–1141.
[69] S.A. Grammatikos, A.S. Paipetis, Compos. Part B 43 (6) (2012) 2687–2696.
[70] A. Vavouliotis, A. Paipetis, V. Kostopoulos, Compos. Sci. Technol. 71 (5) (2011) 630–642.
[71] P. Badrinarayanan, M.K. Rogalski, M.R. Kessler, ACS Appl. Mater. Interfaces 4 (2012) 510–517.
[72] S. Han, J.T. Lin, Y. Aoyagi, D.D.L. Chung, Carbon 46 (7) (2008) 1060–1071.
[73] H. Lee, K. Min, Int. SAMPE Technical Conf., 30th, Materials–The Star at Center Stage (1998) 256–265.
[74] J. Liang, M.C. Saha, M.C. Altan, Procedia Eng. 56 (2013) 814–820.
[75] M. Kistner, R. Watts, A.M. Druma, M.K. Alam, SAMPE Technical Conf., 36th (2004) 11–20.
[76] M. Wrosch, A., Soriano, A.T., Owens, C.D., Russell, J.K., Roberts, J.R. Smith, in: Developing scalable materials and processes for our future, SAMPE Tech. Conf. Exhib., Forth Worth, Texas, October 17–20, 2011, Proc., Vol. 43, Developing Scalable Mat, 2011, pp. Wrosch1/1-Wrosch1/14.
[77] G. Yu, L. Wu, L. Feng, Materials Design 88 (2015) 1063–1070.
[78] H.S. Kim, W. Liu, G. Chen, C.W. Chu, Z. Ren, Proc. Natl. Acad. Sci. 112 (2015) 8205–8210.
[79] X. Zhang, L. Zhao, J. Materiomics 1 (2015) 92–105.
[80] H.J. Goldsmid, Materials 7 (2014) 2577–2592.
[81] S. Feng, S. Li, Q. Luo, H. Fu, Adv. Mater. Res. (Zuerich, Switzerland) 197–198 (Pt. 2, New and Advanced Materials) (2011) 1109–1112.
[82] G. Zhang, Q. Yu, W. Wang, X. Li, Adv. Mater. (Weinheim, Germany) 22 (17) (2010) 1959–1962.
[83] V.H. Guerrero, S. Wang, S. Wen, D.D.L. Chung, J. Mater. Sci. 37 (19) (2002) 4127–4136.
[84] E. Bekyarova, E.T. Thostenson, A. Yu, H. Kim, J. Gao, J. Tang, T. Hahn, T. Chou, M. E. Itkis, R.C. Haddon, Langmuir 23 (2007) 3970–3974.
[85] A. Navarro de Miranda, L.C. Pardini, C.A. Moreira dos Santos, R. Vieira, Mater. Res. 14 (4) (2011) 560–563. http://www.scielo.br/readcube/epdf.php?doi=10.1590/S1516-14392011005000083&pid=S1516-14392011000400022&pdf_path=mr/v14n4/aop_0898-11.pdf&lan=en.
[86] X. An, J. Ma, K. Wang, M. Zhan, J. Appl. Polymer Sci. 133 (9) (2016) 43056, doi: http://dx.doi.org/10.1002/APP.43056.
[87] Y. Lin, M. Gigliotti, M.C. Lafarie-Frenot, J. Bai, J. Reinforced Plastics Compos. 34 (2) (2015) 173–184.
[88] Y. Lin, M. Gigliotti, M.C. Lafarie-Frenot, J. Bai, D. Marchand, D. Mellier, Compos. Part B 76 (2015) 31–37.
[89] J.D. Craddock, D. Qian, C. Lester, J. Matthews, J.P.W. Mansfield, R. Foedinger, M. C. Weisenberger, J. Nanosci. Nanotechnol. 15 (9) (2015) 6852–6855.
[90] K. Li, K. Zhao, Y. Wang, Ceramics Int. 40 (10 Part A) (2014) 15381–15389.
[91] J. Lu, K. Guo, Q. Song, Y. Li, L. Zhang, H. Li, Mater. Design 99 (2016) 389–395.
[92] S. Rechak, C.T. Sun, J. Reinforced Plastics Compos. 9 (6) (1990) 569–582.
[93] M. Guo, X. Yi, Carbon 58 (2013) 241–244.
[94] M. Segiet, D.D.L. Chung, Compos. Interfaces 7 (4) (2000) 257–276.
[95] A. Vlot, L.B., Vogelesang, T.J. De Vries, in: Fiber metal laminates for high capacity aircraft. Int. SAMPE Technical Conf. 30(Materials–The Star at Center Stage), 1998, pp. 456–470.
[96] A.S. Oryshchenko, A.V. Anisimov, V.E. Bakhareva, I.V. Lishevich, Chem. Petrol. Eng. 50 (5–6) (2014) 375–381.
[97] S. Scholz, L. Kroll, Compos. Part B 61 (2014) 207–213.
[98] V.B. Sundaresan, A., Morgan, M. Castellucci, Smart Mater. Res., Hindawi Publishing Corporation, Volume 2013, Article ID 271546, 2013, 12 pages, http://dx.doi.org/10.1155/2013/271546
[99] C. Li, N. Kang, S.D. Labrandero, J. Wan, C. Gonzalez, D. Wang, Ind. Eng. Chem. Res. 53 (3) (2014) 1040–1047.
[100] X. Luo, D.D.L. Chung, Compos. Sci. Technol. 61 (2001) 885–888.
[101] T. Carlson, D. Ordeus, M. Wysocki, L.E. Asp, Compos. Sci. Technol. 70 (7) (2010) 1135–1140.
[102] T. Carlson, L.E. Asp, Compos. Part B 49 (2013) 16–21.
[103] Q. Jiang, R. Yang, G.G. Fu, D.Y. Xie, B. Huang, Z.W. He, Y. Zhao, Mater. Sci. Forum 687 (2011) 158–162.
[104] Z. Jin, Y. Tian, L.J. Su, C.L. Qin, D.Y. Zhao, R.Q. Li, J. Zhao, Adv. Mater. Res. (Durnten-Zurich, Switzerland) 800 (2013) 505–508.
[105] D. Salinas-Torres, J.M. Sieben, D. Lozano-Castello, D. Cazorla-Amoros, E. Morallon, Electrochim. Acta 89 (2013) 326–333.
[106] L.E. Asp, Plastics, Rubber Compos. 42 (2013) 144–149.
[107] E. Jacques, M.H. Kjell, D. Zenkert, G. Lindbergh, M. Behm, M. Willgert, Compos. Sci. Technol. 72 (2012) 792–798.
[108] S. Leijonmarck, T. Carlson, G. Lindbergh, L.E. Asp, H. Maples, A. Bismarck, Compos. Sci. Technol. 89 (2013) 149–157.
[109] T. Pereira, Z. Guo, S. Nieh, J. Arias, H.T. Hahn, J. Compos. Mater. 43 (2009) 549–560.
[110] E. Njuhovic, A. Witt, M. Kempf, F. Wolff-Fabris, S. Gloede, V. Altstaedt, Surf. Coat. Technol. 232 (2013) 319–325.

[111] D. Kwon, P. Shin, J. Kim, K.L. DeVries, J. Park, Polym. Test. 53 (2016) (2016) 293–298.
[112] J. Park, D. Kwon, Z. Wang, J. Byun, H. Lee, J. Park, L.K. Devries, Nanotubes and related nanostructures—2014, Symposium held April 21–25, 2014, San Francisco, California, USA, Mat. Res. Soc. Symp. Proc., Vol. 17002014, pp. 537/1–537/10.
[113] K. Tanaka, H. Koriyama, S. Isshiki, T. Katayama, M. Shinohara, WIT Trans. Built Environment 137(High Performance and Optimum Design of Structures and Materials), (2014) , pp. 283–289.
[114] S. Enoki, K. Kojima, S. Mizuno, K. Katayama, K. Tanaka, WIT Trans.Built Environment 137(High Performance and Optimum Design of Structures and Materials), (2014) , pp. 311–315.
[115] S. Larbi, R., Bensaada, A., Bilek, S. Djebali, in: AIP Conf. Proc. 1653(1, 4th International Congress in Advances in Applied Physics and Materials Science, 2014), 2015, pp. 020066/1-020066/7.
[116] S. Wang, D.P. Kowalik, D.D.L. Chung, Smart Mater. Struct. 13 (3) (2004) 570–592.
[117] R.L. Mazur, P.C. Oliveira, M.C. Rezende, E.C. Botelho, J. Reinforced Plastics Composites 33 (8) (2014) 749–757.
[118] K. Qiao, B. Zhu, X. Gao, C. Di, W. Zhao, X. Yin, Appl. Mechanics Mater. 66-68 (2011) 1072–1077.
[119] H. He, F. Gao, K. Li, Int. J. Mater. Res. (formely Z. Metallkd.) 104 (9) (2013) 899–902.
[120] J. Song, X. Liu, Y. Zhang, B. Huang, W. Yang, J. Appl. Polym. Sci. 133 (13) (2016) 43252.
[121] C. Wang, S. Ying, Fibers Polym. 14 (5) (2013) 815–821.
[122] J. Diaz, L. Rubio, J. Mater. Proc. Technol. 143–144 (2003) 342–346.
[123] Z. Mei, D.D.L. Chung, Thermochim. Acta 369 (1–2) (2001) 87–93.
[124] R.B. Ladani, A.R. Ravindran, S. Wu, K. Pingkarawat, A.J. Kinloch, A.P. Mouritz, R.O. Ritchie, C.H. Wang, Compos. Sci. Technol 131 (2016) 98–109.
[125] N. An, G.P. Tandon, K.V. Pochiraju, Surf. Coat. Technol. 232 (2013) 166–172.
[126] Y. Zhang, X. Lin, W. Chen, H. Cheng, L. Wang, Appl. Surf. Sci. 371 (2016) 504–511.
[127] X. Wang, D.D.L. Chung, Smart Mater. Struct. 5 (1996) 796–800.
[128] S. Wang, D.D.L. Chung, Carbon 44 (13) (2006) 2739–2751.
[129] S. Wang, D.D.L. Chung, J. Mater. Sci. 42 (13) (2007) 4987–4995.
[130] S. Zhu, D.D.L. Chung, Carbon 45 (8) (2007) 1606–1613.
[131] J. Gadomski, P. Pyrzanowski, Mater. Test. 53 (6) (2011) 351–355.
[132] S. Zhu, L. Kong, Z. Li, Y. Lv, Adv. Mater. Res. (Zuerich, Switzerland) 211–212 (Pt. 1, Mechatronics and Materials Processing I) (2011) 480–484.
[133] S. Zhu, J. Li, Z. Li, H. Zheng, Adv. Mater. Res. (Zuerich, Switzerland) 211–212 (Pt. 1, Mechatronics and Materials Processing I) (2011) 421–424.
[134] Z. Mei, D.D.L. Chung, Cem. Concr. Res. 30 (5) (2000) 799–802.
[135] N. Kalashnyk, E. Faulquesc, J. Schjødt-Thomsena, L.R. Jensena, J.C.M. Rauhea, R. Pyrza, Carbon 109 (2016) 124–130.
[136] X. Wang, D.D.L. Chung, Compos. Part B 29B (1) (1998) 63–73.
[137] J. Park, T.K. Hwang, H.G. Kim, Y.D. Doh, Smart Mater. Struct. 16 (1) (2007) 57–66.
[138] J.P. McCrory, S.K. Al-Jumaili, D. Crivelli, M.R. Pearson, M.J. Eaton, C.A. Featherston, M. Guagliano, K.M. Holford, R. Pullin, Compos. Part B 68 (2015) 424–430.
[139] T. Prasse, F. Michel, G. Mook, K. Schulte, W. Bauhofer, Compos. Sci. Technol. 61 (2001) 831–835.
[140] X. Xie, Z. Hong, H. Fan, H. Quan, Z. Li, Adv. Mater. Res. (Durnten-Zurich, Switzerland) 460 (Advanced Materials and Its Application) (2012) 140–144.
[141] N. Angelidis, N. Khemiri, P.E. Irving, Smart. Mater. Struct. 14 (2005) 147–154.
[142] N. Angelidis, P.E. Irving, Compos. Sci. Technol. 67 (2007) 594–604.
[143] S. Wang, D.D.L. Chung, J.H. Chung, Compos. Part A 36 (2005) 1707–1715.
[144] D. Wang, S. Wang, D.D.L. Chung, J.H. Chung, J. Mater. Sci. 41 (8) (2006) 2281–2289.
[145] T.J. Swait, F.R. Jones, S.A. Hayes, Compos. Sci. Technol. 72 (2012) 1515–1523.
[146] X. Luo, D.D.L. Chung, J. Mater. Sci. 35 (19) (2000) 4795–4802.
[147] C. Soutis, Mater. Sci. Eng. A412 (1–2) (2005) 171–176.
[148] M.R. Khosravani, Appl. Mech. Mater 110–116 (Pt. 2, Mechanical and Aerosce Engineering): (2012) 1361–1367.
[149] W. Liu, Z. Chen, X. Cheng, Y. Wang, A.R. Amankwa, J. Xu, Compos. Part B 84 (2016) 33–40.
[150] A.C. Ianasi, IOP Conf. Ser. Mater. Sci. Eng. 95 (1) (2015) 12015–12020.
[151] K. Friedrich, AIP Conference Proceedings 1736(1, 8th Int. Conf. Times of Polymers Composites, 2016) (2016) 020001/1-020001/4.
[152] K. Van Acker, I. Verpoest, J. De Moor, J.-R. Duflou, W. Dewulf, Revue de Metallurgie/Cahiers d'Informations Techniques 106 (12) (2009) 541–546.
[153] H.T. Yin, M.M. Lang, Y.N. Zhao, Appl. Mech. Mater. 454 (2014) 263–267.
[154] L.C. Hollaway, J. Compos. Constr. 15 (2) (2011) 239–247.
[155] L. Sun, Z. Deng, Adv. Mater. Res. (Durnten-Zurich, Switzerland) 341–342 (Pt. 1, Material and Manufacturing Technology II) (2012) 173–176.
[156] B. Wang, J.Q. Liu, Y.S. Liu, Y. Dou, Appl. Mech. Mater. 473 (Mechanical Engineering, Intelligent System and Applied Mechanics) (2014) 111–115.
[157] A. Daliri, W.S.T. Rowe, K. Ghorbani, A. Galehdar, C.H. Wang, S. John, Materials Australia: Mag. Eng. Mater. Technol. 45 (4) (2012) 34–36.
[158] M. Klebor, O. Reichmann, E.K. Pfeiffer, A. Ihle, S. Linke, C. Tschepe, S. Roeddecke, I. Richter, M. Berrill, J. Santiago-Prowald, European Space Agency, [Special Publication] SP-691 (Proc. 12th European Conf. Spacecraft Structures, Materials & Environmental Testing, 2012) (2012) a10/1–a10/6.
[159] A. Szarek, P. Postawa, Kompozyty 10 (1) (2010) 46–51.
[160] http://inhabitat.com/kengo-kuma-anchors-an-earthquake-resistant-building-with-carbon-fiber-threads/. (as viewed on Aug. 31, 2016).
[161] U. Meier, Arabian J. Sci. Eng. 37 (2) (2012) 399–411.
[162] http://www.compositesworld.com/news/carbon-fiber-grids-replace-steel-in-facade-panels. (as viewed on Aug. 31, 2016).
[163] http://altusprecast.com/products/c-grid/. (as viewed on Aug. 31, 2016). http://worldindustrialreporter.com/new-research-report-predicts-11-9-cagr-global-carbon-fiber-market-2019/. (as viewed on 8/31/2016).
[164] http://www.fortressstabilization.com/concrete-reinforcement.php. (as viewed on Aug. 31, 2016).
[165] http://www.compositesworld.com/blog/post/composites-help-to-repair-earthquake-damaged-bridges. (as viewed on Aug. 31, 2016).
[166] X. Luo, D.D.L. Chung, Compos. Part B 30 (3) (1999) 227–231.
[167] S. Zhai, W. Jiang, L. Wei, H.E. Karahan, Y. Yuan, A.K. Ng, Y. Chen, Mater. Horizons 2 (6) (2015) 598–605.
[168] A.D. Jagadale, G. Guan, X. Du, X. Hao, X. Li, A. Abudula, RSC Adv. 5 (70) (2015) 56942–56948.
[169] M.M.B. Hasan, A. Nocke, C. Cherif, J. Appl. Polym. Sci. 130 (2) (2013) 1179–1184.
[170] D. Zhang, Y. Zhang, Y. Luo, P.K. Chu, Nano Energy 13 (2015) 47–57.
[171] M.A.I. Shuvo, H. Karim, M.D. Rajib, D. Delfin, Y. Lin, Proc. SPIE 9058(Behavior and Mechanics of Multifunctional Materials and Composites) (2014) 905808/1–905808/7.
[172] D.A. Griffin, SAMPE Conf. Proc. 54 (2009) (griff1/1-griff1/21).
[173] D.A. Griffin, SAMPE J. 45 (5) (2009) 6–16.
[174] H. Onikura, T. Sajima, Annual Report of the Faculty of Engineering, Kyushu University, 2005, pp. 24–30.
[175] O. Anil, C.M. Belgin, Sci. Eng. Compos. Mater. 15 (2) (2008) 141–158.
[176] H. Carr, A. Allan, Ann. Tech. Conf. –Soc. Plastics Eng. 67th (2009) 2253–2258.
[177] H. Toutanji, M. Han, E. Ghorbel, J. Compos. Constr. 16 (1) (2012) 35–46.
[178] M. Chini, R. Antonsen, O. Vennesland, B. Arntsen, J.H. Mork, 2007 RILEM Proc PRO 56 (Integral Service Life Modelling of Concrete Structures) (2007) 395–402.
[179] M. Lee, S. Kim, H. Kim, O. Lim, C. Kang, Proc. Inst. Mech. Eng., Part B: J. Eng. Manuf. 229 (1) (2015) 86–99.
[180] A.K. Patnaik, C.L. Bauer, T.S. Srivatsan, Sadhana 33 (3) (2008) 261–272.
[181] J. Tomioka, K. Kiguchi, Y. Tamura, H. Mitsuishi, Int. J. Hydrogen Energy 36 (3) (2011) 2513–2519.
[182] http://www.zoltek.com/carbonfiber/the-future-of-carbon-fiber/. (viewed on Aug. 31, 2016).
[183] N. Saito, K. Aoki, Y. Usui, M. Shimizu, K. Hara, N. Narita, N. Ogihara, K. Nakamura, N. Ishigaki, H. Kato, H. Haniu, S. Taruta, Y.A. Kim, M. Endo, Chem. Soc. Rev. 40 (7) (2011) 3824–3834.
[184] C. Li, X. Cui, Z. Wu, J. Zeng, S. Xing, Adv. Mater. Res. (Durnten-Zurich, Switzerland) 774–776(Advanced Technologies in Manufacturing, Engineering and Materials) (2013) 1322–1325.
[185] C.D. Warren, F.L. Paulauskas, F.S. Baker, C.C. Eberle, A. Naskar, SAMPE J. 45 (2) (2009) 24–36.
[186] D.A. Baker, T.G. Rials, J. Appl. Polym. Sci. 130 (2) (2013) 713–728.
[187] https://www.ornl.gov/sites/default/files/LowCostCarbonFiber_ProcessBrochure_Final.pdf. U.S. Patent Application 62/273,559 (as viewed on Aug. 31, 2016).
[188] http://worldindustrialreporter.com/new-research-report-predicts-11-9-cagr-global-carbon-fiber-market-2019/. (as viewed on Aug. 31, 2016).
[189] L. Xiao, D.D.L. Chung, Carbon 108 (2016) 291–302.
[190] P. Kumar, P.M. Mohite, S. Kamle, Arch. Mech. 65 (1) (2013) 27–43 (93).